Nucleic Acids Research, 2025, **53**, gkaf504
https://doi.org/10.1093/nar/gkaf504
Gene regulation, Chromatin and Epigenetics

Nat10 maintains the homeostasis of pluripotent and 2-cell-like states in mouse embryonic stem cells through mRNA cytidine acetylation

Guofeng Feng[1,2,†], Guoxing Yin[1,2,†], Yusheng Liu[3,4,†], Chang Liu[1,2], Jie Li[1,2], Jiangtao Lu[1,2], Yongqin Yu[1,2], Ziyi Jin[1,2], Yiwei Wu[1,2], Yanbin Yue[4,5], Xiufang Gao[4], Jiaqiang Wang[5], Falong Lu[4], Lin Liu[1,2,*]

[1]State Key Laboratory of Medicinal Chemical Biology, Nankai University, 94 Weijin Road, Tianjin 300071, China
[2]Department of Cell Biology and Genetics, Nankai University, 94 Weijin Road, Tianjin 300071, China
[3]College of Life Science, Northeast Forestry University, Harbin 150040, China
[4]State Key Laboratory of Molecular Developmental Biology, Institute of Genetics and Developmental Biology, Chinese Academy of Sciences, Beijing 100101, China
[5]College of Life Science, Northeast Agricultural University, Harbin 150006, China

[*]To whom correspondence should be addressed. Email: liulin@nankai.edu.cn
[†]These authors contributed equally to this work.

Abstract

Naïve mouse embryonic stem cells (mESCs) are characterized by a mixed population of cells in an interconvertible pluripotent state and a totipotent 2-cell (2C)-like state. It remains to be understood how the pluripotent state is maintained while the 2C-like state is suppressed. We show that *N*-acetyltransferase 10 (Nat10) maintains the pluripotent state and suppresses the 2C-like state in mESCs through mRNA modification and stabilization. Nat10 as a nucleolar protein may indirectly interact with heterochromatin through Ncl. Nat10 catalyzes the N^4-acetylcytidine (ac^4C) modification of mRNAs encoding the key pluripotency genes including *Oct4*, *Esrrb* and *Zfp42* and enhances their mRNA stability, thus increasing their protein levels for pluripotency. Moreover, Nat10 acetylates and stabilizes heterochromatin modifiers such as *Kap1* mRNA and protein to repress the 2C genes by maintaining the H3K9me3 complex. Together, these findings highlight critical roles for Nat10 in maintaining the pluripotency network and repressing the 2C-like program via mRNA ac^4C modification, providing insights into the transition between pluripotent and totipotent states in mESCs.

Graphical abstract

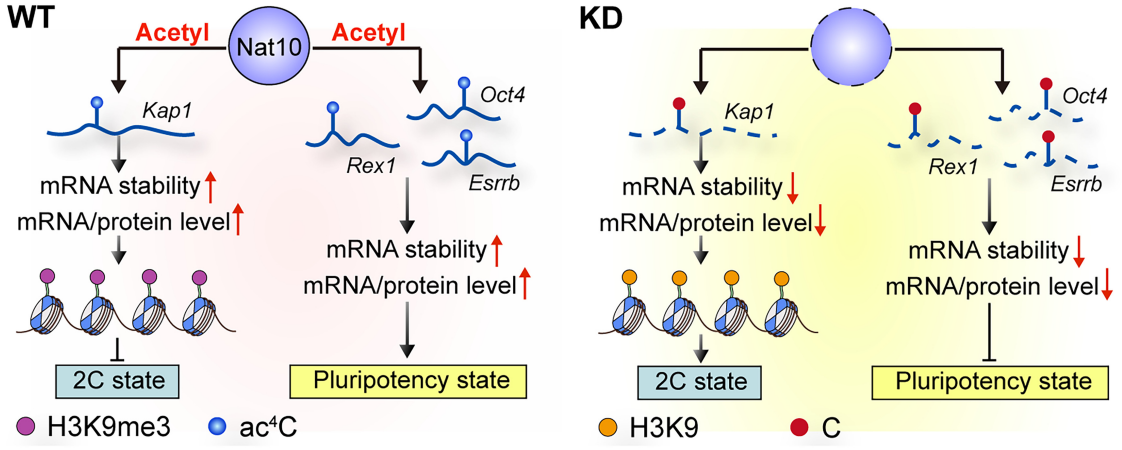

Introduction

N-acetyltransferase 10 (NAT10) is a multifunctional enzyme involved in various cellular processes, including RNA modification, the DNA damage response, and cell cycle regulation. One of its primary roles is catalyzing the formation of N^4-acetylcytidine (ac^4C) in RNA, a highly conserved

Received: November 27, 2024. **Revised:** May 22, 2025. **Editorial Decision:** May 23, 2025. **Accepted:** May 28, 2025

posttranscriptional modification [1]. ac^4C modification is found in multiple types of RNA, including mRNAs, tRNAs, and rRNAs [2, 3], and plays critical roles in enhancing RNA stability, translation efficiency, and fidelity [1, 4]. NAT10-mediated ac^4C modifications have been linked to various biological processes, such as cellular stress responses, development, and differentiation. Targeting *NAT10* for knockdown (KD) can extend the lifespan of mice [5], and ac^4C modification plays an important role in the maturation of mouse oocytes [6]. Dysregulation of NAT10 and ac^4C levels has been associated with diseases, including cancer and neurodegenerative disorders; currently, many studies have shown that Nat10 can be used as an intervention target for many tumor-related targets [7–12], and that inhibition of Nat10 can improve survival.

NAT10 also plays a critical role in human embryonic stem cells (hESCs). It regulates pluripotency by modulating gene expression patterns and mRNA stability, and loss of NAT10 function impairs hESC self-renewal and differentiation potential [13]. In addition, NAT10 has been reported to be an important regulator of pluripotent reprogramming and differentiation in hESCs [14], highlighting the essential role of NAT10 in maintaining stem cell identity and developmental capacity. However, the functions of Nat10 and ac^4C modifications in mouse embryonic stem cells (mESCs) are still unknown.

mESCs are a classical type of pluripotent cell established from the inner cell mass (ICM) of blastocysts or early embryos under appropriate culture conditions *in vitro* [15, 16]. mESCs have the ability to self-renew indefinitely and the potential to differentiate into all cell types in the body. A small population of cells (1%–5%) within mESCs cultures shares the transcriptional and proteomic features of 2C embryos and displays strikingly different patterns of pluripotency markers from the majority of (95%–99%) mESCs [17–21]. Significant progress has been made in understanding the epigenetic mechanisms underlying the regulation of 2C gene expression in mESCs [22–24].

The 2C stage of mouse embryonic development is characterized by extensive epigenetic reprogramming, including DNA methylation, histone modifications, chromatin accessibility and epitranscriptomic-related RNA modifications. For example, DNMT3B, a type of DNA methyltransferase (DNMT), plays a critical role in regulating the expression of key transcription factors, such as Sox2 [25]. Moreover, the ten-eleven translocation (TET) family methylcytosine hydroxylase TET1/TET2 physically associates with NANOG and activates other important pluripotent factors, such as OCT4 [26, 27]. Pioneer transcription factors, such as Dux, play crucial roles in activating 2C genes by increasing chromatin accessibility [28]. Additional factors, including DPPA2, DPPA4, and NELFA, interact with Dux and enhance its activity. These interactions facilitate the transition of mESCs to 2C-like cells (2CLCs) by modulating chromatin accessibility and gene expression [29, 30]. In contrast, Rif1 is highly and specifically expressed in mESCs [31] and intriguingly suppresses 2C genes, such as *Zscan4* and *Tcstv1/3*, to maintain telomere length homeostasis in mESCs by stabilizing H3K9me3 complexes [19]. The histone H3K9 methyltransferase SETDB1 is an essential factor for embryonic development and pluripotent ICM establishment [20]. Additionally, rRNA biogenesis regulates the transition of mESCs to 2CLCs by reorganizing the 3D structure of perinucleolar heterochromatin. Inhibition of rRNA synthesis triggers nucleolar stress, which leads to changes in heterochromatin and the activation of 2C genes [32]. Another factor, LIN28, is involved in promoting nucleolar/ribosomal functions while repressing the 2C-like transcriptional program in mESCs [33]. METTL3, the methyltransferase for m^6A RNA modification, suppresses *ERV* transcription and maintains genomic stability, thereby influencing 2C gene expression [34]. FTO, a m^6A demethylase, can mediate m^6A demethylation of long interspersed element-1 (*LINE1*) RNA in mESCs, which regulates embryonic development [35].

Here, we first identify Nat10 as a new player in the 2C program and report the mechanism by which Nat10 balances the pluripotent and 2C-like states via ac^4C RNA modification in mESCs.

Material and methods

Cell culture

E3 and E14 mESCs were used in this study. E3 mESCs were cultured on mitomycin C-inactivated MEF feeder cells [36]. E14 mESCs were cultured on 0.2% gelatin (Sigma). The culture medium of the mESCs consisted of 15% FBS (ES quality, HyClone) supplemented with penicillin (100 U/ml) and streptomycin (100 μg/ml) (Gibco), nonessential amino acids (Gibco), 1 mM L-glutamine (Gibco), 0.1 mM β-mercaptoethanol (Sigma), mLIF (1000 U/ml) (ESGRO, Chemicon), and Knock-out DMEM (Gibco). mESCs were cultured in a sterile incubator at 37°C in 5% CO_2.

Generation of *Nat10* KD ESCs

The *Nat10* KD cells were generated via the PiggyBac (PB)-mediated transgene of an inducible artificial miRNA targeting *Nat10* with the miR155 backbone. Briefly, a PB transgene vector carrying inducible artificial miRNAs (TGAATTTCAAGACAGCTTTGG; AACACATTGACCCTGATCACC; and ATGAGAAGCCACATAGAGAGC) was transfected into E14 mESCs together with a vector carrying PBase and a vector carrying the puromycin resistance gene via LIPOFECTAMINE 3000. The surviving clones after puromycin treatment were selected and screened for successful *Nat10* KD after doxycycline treatment via western blotting. Two independent clones with successful *Nat10* KD after doxycycline treatment were retained for further study.

Vector construction

The murine *Nat10* and *Kap1* CDSs were subsequently cloned and inserted into the OE-3 × flag vector (gift from the Lingyi Chen laboratory). Stable cell lines were established from single clones after 7–10 days of selection with 2 μg/ml puromycin.

Mutation of Nat10

The 641 glycine site of Nat10 is considered the catalytic activity center of Nat10. The G641E mutant is often used as a catalytically dead model [37]. The mutated bases were introduced into the primers listed below, followed by overlap extension PCR to amplify the DNA encoding *Nat10* containing the mutated sites ($Nat10^{G641E}$).

Mutant-F: ttatcaagggatgggatatgagagccgagcgct

Mutant-R: gcagcgctcggctctcatatcccatcccttgataa

Rescue experimental design

The *iNat10; Nat10*-KD mESCs were first cultured for 48 h in the presence of Dox (1 μg/ml); at this point, the Nat10 protein level obviously decreased, and the cells presented a differentiated phenotype. Then, exogenous *Nat10* full-length (*Nat10* FL) or *Nat10* catalytic mutant ($Nat10^{G641E}$) was transfected into these cells via LIPOFECTAMINE 3000 for transient overexpression, after which the cells were cultured for another 48 h. Finally, samples called rescued cells for 2C state and pluripotent state marker detection were collected.

Western blot

Protein extracts were prepared with NP40 lysis buffer supplemented with the protease inhibitor PMSF and cocktail. The prepared protein samples were subjected to 10% Acr-Bis sodium dodecyl sulphate-polyacrylamide gel electrophoresis (SDS-PAGE) and transferred to polyvinylidene difluoride (PVDF) membranes (Millipore). The transferred PVDF membrane was blocked with 5% nonfat milk at room temperature for 2 h. The primary antibody was incubated with the transferred membrane at 4°C overnight, and the secondary antibody incubated at room temperature for 1 h. The protein band was visualized via Supersignal West Pico Chemiluminescent Substrate (Millipore). The antibodies used included rabbit anti-Nat10 (1:1000, Abcam, ab194297), rabbit anti-Actin (1:50,000, ABclonal, AC026), rabbit anti-Zscan4 (1:1000, Sigma−Aldrich, AB4340), rabbit anti-Kap1 (1:2000, GeneTex, GTX102226), rabbit anti-Nucleolin (1:2000, CST, 14574S), mouse anti-Oct4 (1:500, Santa Cruz, sc-5279), rabbit anti-Nanog (1:1000, Abcam, ab80892), rabbit anti-Suv39h1 (1:1000, 14574S), mouse anti-Hp1α (1:500, Sigma-Aldrich, 05–689), mouse anti-Setdb1 (1:1000, Abcam, ab107225), rabbit anti-Hp1γ (1:1000, Novus, NBP2-15736), rabbit anti-Suv39h1 (1:1000, Abcam, ab283262), rabbit anti-H3K9me3 (1:1000, Abcam, ab8898), rabbit anti-H3K9ac (1:1000, Abcam, ab4441), rabbit anti-H3K27ac (1:1000, Abcam, ab177178), and rabbit anti-H3 (1:5000, Abcam, ab1791) antibodies. The secondary antibodies goat anti-rabbit IgG (H + L) (GeneScript, A00098) or goat anti-mouse IgG (H + L) (GeneScript, A00160) were diluted 1:50,000.

Co-immunoprecipitation (Co-IP)

The cells were cotransfected with epitope-tagged expression plasmids. Forty-eight hours after transfection, the cells were harvested with 500 μl of lysis buffer (20 mM Tris-HCl, pH = 8.0; 100 mM NaCl; 0.5% NP-40; and 1 mM EDTA) supplemented with protease inhibitor cocktail (#04693132001, Roche) and PMSF (#PB0425). The cell lysate was rotated at 4°C for 30 min. After centrifugation at 13,000 × g for 10 min, the supernatants were used for immunoprecipitation (IP). The cell extracts were incubated with anti-Flag antibody (F1804 Sigma) overnight at 4°C, followed by incubation with lysis buffer and washing with 50 μL of protein G agarose resin (Yeasen, 36405ES08) for 3 h. The incubated protein G was washed with lysis buffer at 4°C for 10 min. The cell extracts (50 μL of input) and IP samples were resuspended in 80 μL of SDS buffer, followed by pipetting up and down several times to mix the samples. The sample was boiled for 5 min and then subjected to Western blotting with an anti-Flag (1:2000, Sigma, F1804) antibody to detect protein−protein interactions.

Mass spectrometry

For mass spectrometry analysis of heterochromatin-associated proteins and murine Nat10-associated proteins, the immunoprecipitate was subjected to 10% Acr-Bis SDS-PAGE and separated approximately 2 cm from the well. The gel was cut and used for mass spectrometry analysis by the PTM BIO Company (Hangzhou, China).

Real-time qPCR for mRNA quantification

Total RNA was prepared with TRIzol (Invitrogen, Carlsbad, CA, USA), and the concentration of total RNA was determined with a NanoDrop 2000 (Thermo Scientific). One microgram of RNA was reverse transcribed to cDNA via M-MLV reverse transcriptase (Thermo Scientific, 28025021). Real-time quantitative PCR (qPCR) was performed in duplicate with FS Universal SYBR Green Master Mix (Roche) and run on an iCycler MyiQ2 detection system (Bio-Rad). Each sample was set up in duplicate and normalized to *Gapdh*. qPCR data were analyzed via the ΔΔCt method. The 2C genes and 18S rRNA and 28S rRNA primers used were previously described [32]. All the primers used for qPCR analysis are listed in Supplementary Table S1.

Immunofluorescence microscopy

mESCs were fixed at 4°C for 30 min in 3.7% paraformaldehyde (PFA) in phosphate-buffered saline (PBS), washed three times with PBS, and permeabilized in 0.1% Triton X-100 in blocking solution (3% goat serum plus 0.1% BSA in PBS) for 30 min at room temperature and sealed at room temperature for 2 h. The primary antibody was incubated overnight at 4°C, and the secondary antibody was incubated at room temperature for 1 h. The antibodies used were as follows: rabbit anti-Nat10 (1:150), rabbit anti-Nucleolin (1:200), mouse anti-Flag (1:200), rabbit anti-Zscan4 (1:400), and mouse anti-Hp1α (1:150). mESCs were washed three times (15 min each) with PBS and incubated for 2 h with secondary antibodies at room temperature. Goat anti-mouse IgG (H + L) FITC (115–095-003, Jackson), goat anti-rabbit IgG (H + L) Alexa Fluor 594 (111–585-003, Jackson), and rabbit IgG/Alexa Fluor 647 (bs-0295P-AF647, Bioss) were diluted 1:200 with blocking solution. Samples were washed and counterstained with 0.5 μg/mL DAPI in Vectashield mounting medium (Vector Laboratories). The fluorescence was detected and imaged via an Axio Imager Z2 fluorescence microscope (Zeiss).

RNA stability assay

Nat10 CON and *Nat10* KD mESCs were treated with actinomycin D (MCE, HY-17559) at a final concentration of 5 μg/ml for the indicated times (0, 1, 4, and 8 h) and collected. Total RNA was extracted with TRIzol (Invitrogen, Carlsbad, CA, USA) and analyzed via RT-qPCR. The half-life of the mRNA was calculated according to a previously reported method [38].

Dot blot assay of RNA ac^4C acetylation

Dot blotting was performed as previously described [1]. Briefly, 2 μg of RNA was denatured at 95°C for 5 min, immediately placed on ice for 1 min, loaded onto Hybond-N + membranes and crosslinked with UV crosslinkers. Unbound mRNA was washed with gentle shaking for 5 min. Next, the membranes were incubated in 20 mL of blocking

buffer (5% skim milk powder) for 2 h at room temperature with gentle shaking and then placed in anti-ac^{4}C antibody dilution buffer (1:200, Abcam, ab252215) at 4°C overnight. The membranes were subsequently washed three times in wash buffer for 15 min each time and then incubated with 2 mL of goat anti-rabbit IgG antibody (H + L) (1:50,000, GeneScript, A00098) for 1 h at room temperature. The membranes were gently washed three times in wash buffer for 15 min each time. The results were visualized using Supersignal West Pico Chemiluminescent Substrate (Millipore). For internal standard detection, the membranes were incubated with 0.02% methylene blue (Sigma–Aldrich) in 0.3 M sodium acetate (pH 5.2) for 10 min and then washed with ddH_2O.

RNA-seq library construction and sequencing

mRNA was purified from total RNA via poly-T oligo-attached magnetic beads. Fragmentation was carried out using divalent cations under elevated temperature in NEBNext First Strand Synthesis Reaction Buffer (5×). First-strand cDNA was synthesized via DNA polymerase I and RNase H. The remaining overhangs were converted into blunt ends via exonuclease/polymerase activities. After adenylation of the 30 ends of the DNA fragments, NEB Adaptors with hairpin loop structures were subsequently ligated to prepare for hybridization. To select cDNA fragments of preferentially 150–200 bp in length, the library fragments were purified with AMPure XP random hexamer primers (Beckman Coulter, Beverly, USA) and M-MLV Reverse Transcriptase (RNase H). Second-strand cDNA synthesis was subsequently performed using DNA Polymerase I and RNase H. Then, 3 μL of USER Enzyme (NEB, USA) was used with size-selected and cDNA adaptors ligated at 37°C for 15 min, followed by 5 min at 95°C prior to PCR. PCR was performed with Phusion High-Fidelity DNA polymerase, universal PCR primers and Index Primer. Finally, the PCR products were purified via the AMPure XP system, and library quality was assessed via the Agilent Bioanalyzer 2100 system. Clustering of the index-coded samples was performed on a cBot Cluster Generation System via the TruSeq PE Cluster Kit (Illumina) according to the manufacturer's instructions. After cluster generation, the library preparations were sequenced on an Illumina HiSeq platform by Annoroad Gene Technology (Beijing, China).

Acetylated RNA immunoprecipitation sequencing (ac^{4}C-RIP-seq)

The acRIP-Seq service was provided by CloudSeq Biotech Co., Ltd. (Shanghai, China). The RNA was first extracted from the *Nat10* CON and *Nat10* KD mESCs by TRIzol, the RNA was quality controlled, and the concentration and purity of the RNA detected. Total RNA was subjected to immunoprecipitation with the GenSeq® ac^{4}C RIP Kit (GenSeq Inc.) following the manufacturer's instructions. Briefly, RNA was randomly fragmented into approximately 200 nt fragments via RNA fragmentation reagents. Protein A/G beads were coupled to the ac^{4}C antibody by rotation at room temperature for 1 h. The RNA fragments were incubated with the bead-linked antibodies and rotated at 4°C for 4 h. After incubation, the RNA/antibody complexes were washed several times, and then, the captured RNA was eluted from the complexes and purified. The RNA libraries for the IP and input samples were then constructed with the GenSeq® Low Input Whole RNA Library Prep Kit (GenSeq, Inc.) following the manufacturer's instructions. Libraries were qualified via an Agilent 2100 bioanalyzer (Agilent) and then sequenced on a NovaSeq platform (Illumina).

Chromatin immunoprecipitation sequencing (ChIP-seq)

ChIP-seq was performed as previously described [39]. Briefly, approximately 2 × 10^7*Nat10* CON and *Nat10* KD mESCs were first fixed with 1% PFA and then lysed and sonicated to obtain the majority of the DNA fragments at 100–500 bp. DNA fragments were then enriched via immunoprecipitation with 5 μg of H3K9me3 antibody (ab8898, Abcam) or 10 μg of RNA Pol II (39497, Active Motif) and Dynabeads M280 (Life Technologies) and rocked at 4°C overnight. The immunoprecipitated material was eluted from the beads by heating for 30 min at 65°C. The samples were subsequently incubated at 65°C overnight for reverse crosslinking. The samples were then extracted with phenol:chloroform:isoamyl alcohol (25:24:1, pH > 7.8), followed by the addition of chloroform, ethanol precipitation in the presence of glycogen, and resuspension in ddH_2O. ChIP-enriched DNA was used for ChIP–qPCR analysis or library construction by Novogene Corporation. Each library was subsequently sequenced, resulting in ∼20 million reads (125 bp). The primers used for ChIP–qPCR analysis are listed in Supplementary Table S2.

RNA-seq analysis

The clean reads were first aligned to the mouse reference genome (mm10) via STAR software [40] with the default parameters. Expression matrix was generated by Featurecounts software [41]. DEGs were calculated via the R package DEseq2 [42], and the expression levels were represented by the CPM. DEGs were defined on the basis of the fold change in expression levels and false discovery rate (FDR) value. If the absolute fold change was greater than 2 and the FDR value was less than 0.05, genes were considered to be differentially expressed. To compare the functions of the DEGs, we used the Metascape website (https://metascape.org/gp/index.html#/main/step1).

ChIP-seq analysis

For ChIP-seq data analysis, the clean ChIP-seq reads were aligned to the mouse genome assembly (mm10) via BOWTIE2 [43] with the parameter "–local -k 1". This setting ensures that if more than one equivalent best alignment was found, only one of those hits would be randomly reported. Therefore, instead of excluding reads from repetitive elements, multiple-hit reads are evenly distributed over highly similar repeat elements across the genome. Bam files were obtained via SAMtools (v.1.7). The ChIP-seq peaks were called with MACS2 (v.2.2.7.1). Signal tracks for each sample were generated via the bamCompare function of deeptools and normalized by calculating the reads per kilobase of transcript per million mapped reads (RPKM) [44]. Scatterplots, correlation plots, and heatmaps are displayed via deepTools [45]. Figures illustrating these continuous tag counts over selected genomic intervals were created in the IGV browser [46].

acRIP-seq analysis

Clean reads were aligned to the reference genome (mm10) via HISAT2 software (v.2.2.1) [47]. The aligned SAM-

format reads were sorted, transformed to BAM format, and indexed via SAMtools (v.1.7). Finally, the BAM-format reads for each paired IP + input sample were processed via exome-Peak2 software (http://bioconductor.org/packages/release/bioc/html/exomePeak2.html, v1.8.1) to identify significant acetylation peaks in each IP sample [48]. HOMER software was used for de novo discovery of the acetylation motif [49]. The distribution of ac^4C peaks along the transcripts was characterized via the R package Guitar [50]. Interval annotation analysis of ac^4C peaks along the transcripts was performed via the R package ChIPseeker [51]. Visualization of the ac^4C peaks per-base coverage across the genome was performed via the Integrative Genome Viewer (IGV) [46].

To compare the functions of the peaks, we used the Metascape website (https://Metascape.org/gp/index.html#/main/step1).

Statistical analysis

The data are presented as the means ± SEMs. Statistical analyses were performed via an unpaired two-tailed Student's *t* test in PRISM software (version 10.2.0) to compare the differences between the treatment and control groups, assuming equal variance. Two-way ANOVA with Tukey's test was used for comparisons of more than two groups. *, **, *** and **** indicate $P < 0.05$, $P < 0.01$, $P < 0.001$ and $P < 0.0001$, respectively; ns, no significant difference.

Results

Nat10 may indirectly interact with heterochromatin

To further identify heterochromatin-associated proteins in mESCs, we enriched heterochromatin following an established method [52] and subjected it to immunoprecipitation with an anti-H3K9me3 antibody followed by mass spectrometry (IP–MS). Known heterochromatin-associated proteins, such as Cbx1, Cbx3, Cbx5, Dnmt3a, Dnmt3l, and Npm1, were identified (Fig. 1A and Supplementary Table S4), which indicates successful enrichment of heterochromatin-associated proteins. Next, we compared our data with data from Becker *et al*. (2017) [52] to validate the method used in our project. We also compared with the known heterochromatin-associated proteins identified in mESCs by Ji *et al*. (2015) [53], and noted that Nat10 could be a potential candidate heterochromatin-associated protein by following Becker *et al*. in mESCs (Fig. 1A).

We expressed 3 × *Flag-Nat10* fusion protein in mESCs. In addition to the Flag-Nat10 overexpressing mESCs, we also transfected the empty Flag vector (Flag_EV) into mESCs. We then performed immunoprecipitation mass spectrometry (IP–MS) with an anti-Flag antibody in the two independent mESC cell lines (Fig. 1B and Supplementary Fig. S1A). If the unique peptides were identified in two or more repeats, we assumed that the protein was present. Under these conditions, we identified 341 proteins in the FLAG_Nat10_IP samples and 188 proteins in the Flag_EV_IP samples (Supplementary Tables S5 and S6). The 119 proteins are shared between the two datasets. By removing the background proteins, the additional 222 proteins in the FLAG_Nat10_IP samples were considered as potentially being interacted with Nat10 (Fig. 1C and Supplementary Table S7).

Notably, Nat10 is associated with the known interactors Tardbp and Thumpd1 [54, 55] or with histone components such as H3f3a, H1f2 and H2bc3 (Fig. 1D). GO enrichment analysis of these proteins revealed that most of the enriched terms were related to the ribosome and spliceosome (Fig. 1E), which play important roles in determining the cell fate of mESCs [32, 56]. These findings suggest that Nat10 may play important roles in mESCs. When the heterochromatin-associated proteins and Nat10-interacting proteins were compared, approximately one-third of the proteins identified via Flag/Nat10-IP-MS were also heterochromatin-associated proteins. These proteins were enriched mostly in biological processes related to translation or ribosome biogenesis (Supplementary Fig. S1B and C). Furthermore, we performed Co-immunoprecipitation (Co-IP) with anti-Flag and showed that Flag-Nat10 was associated with Ncl but did not interact with H3K9me3 methyltransferases such as Suv39h1 and Setdb1, nor with H3K9me3 binding protein Kap1 or heterochromatin-binding protein, Hp1α and Hp1γ (Supplementary Fig. S1D). Similar protein interaction results were obtained via Co-IP with endogenous NAT10 in the HEK293T cell line (Supplementary Fig. S1E). Immunofluorescence revealed that Flag fully colocalized with Nat10 in Flag-Nat10-transfected mESCs (Fig. 1F). Nat10 almost completely colocalized with Ncl and partly colocalized with Hp1α (Fig. 1G). In addition, Nat10 was located on or near heterochromatin regions at the interphase stage and resided at the periphery of the condensed chromosomes with the breakdown of nucleoli when nocodazole was used to partially arrest the mESCs at metaphase (Fig. 1H).

We also performed co-immunofluorescence of Nat10 with Hp1α, a heterochromatin-binding protein at the interphase and metaphase stages. Interestingly, during the metaphase stage, the foci of Hp1α were disordered, and Nat10 resided at the periphery of the condensed chromosomes (Supplementary Fig. S1F, left four panels). Moreover, we performed co-immunofluorescence in *Nat10*-overexpressing mESCs by using H3K9me3 and *Nat10*-Flag, which can indicate the Nat10 expression pattern. The heterochromatin H3K9me3 foci were also reduced at the metaphase stage, and the *Nat10*-Flag was located around the 4′,6-diamidino-2-phenylindole (DAPI) chromosome region (Supplementary Fig. S1F, right four panels).

The dynamic distribution of Nat10 is also consistent with observations in Saos-2 cells [57], indicating that Nat10 is associated with chromosomes at different cell cycle stages. These data suggest that Nat10 could be indirectly associated with heterochromatin in mESCs.

Nat10 is required for maintaining the pluripotency of mESCs

We compared the Nat10 expression levels between mESCs and somatic cells. The Nat10 level in mESCs was much greater than that in mouse embryonic fibroblasts (MEFs) (Supplementary Fig. S2A–C), suggesting that Nat10 may have a role in mESCs. We also analyzed the expression level of *Nat10* between mESCs in different states of pluripotency via our previous data [58] and showed that *Nat10* expression was lower in primed state cells than in naïve state cells (Supplementary Fig. S2D), which implied that Nat10 may play important roles in naïve state mESCs. To study the potential functions of Nat10 in mESCs, we constructed doxycycline (Dox)-inducible *Nat10*-KD mESCs, termed *iNat10; Nat10*-KD ESCs. The *iNat10; Nat10* KD ESCs cultured for 48 h in

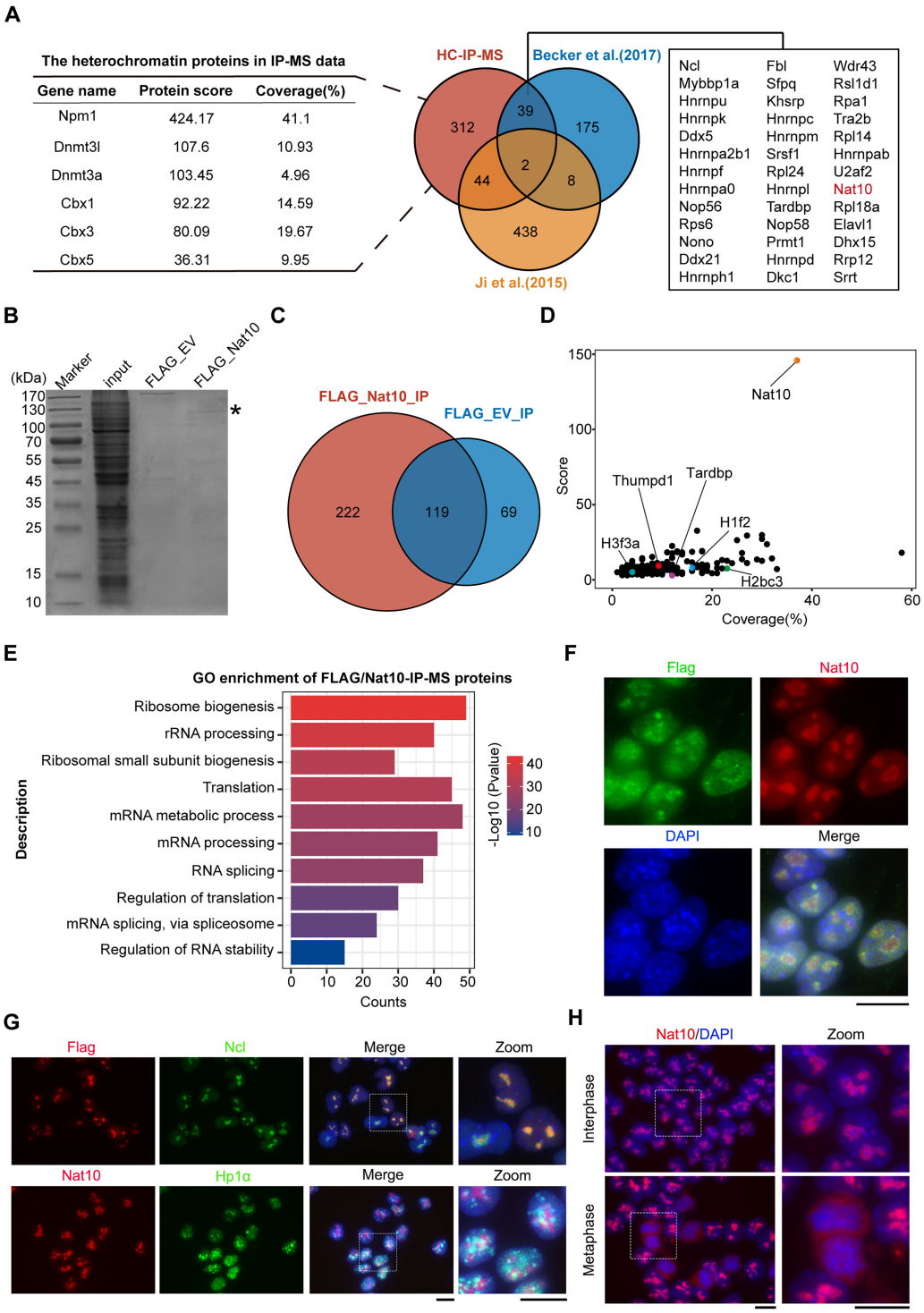

Figure 1. Nat10 may indirectly interact with heterochromatin. (**A**) Venn diagram showing heterochromatin-associated proteins in our heterochromatin-IP-MS data (HC-IP-MS) and data from Becker *et al.* (2017) and Ji *et al.* (2015). In total, 397 proteins were identified as potential heterochromatin-associated proteins. Known heterochromatin-associated proteins are shown on the left, and Nat10 is a potential heterochromatin-associated protein shown on the right. (**B**) Coomassie brilliant blue staining of the Flag/Nat10-interacting proteins that were immunoprecipitated from 3× *Flag-Nat10*-overexpressing (OE) mESCs and identified via mass spectrometry. The molecular weights (MWs) are shown on the left of the gel. The putative Nat10 protein is indicated. (**C**) Venn diagram showing Nat10 potential interactors between FLAG_Nat10_IP samples (left circle) and Flag_EV_IP samples (right circle). A total of 222 proteins in the FLAG_Nat10_IP samples were considered to potentially interact with Nat10. (**D**) Scatter plot showing the Nat10-immunoprecipitation mass spectrometry (IP-MS) results. Highlights indicate some histone components such as H1f2 and H3f3a and the known Nat10 binding protein Tardbp and Thumpd1 and other potential binding proteins. (**E**) Functional enrichment analysis for genes marked by the Nat10-interacting proteins identified by IP–MS. (**F**) Immunofluorescence images of the Nat10 antibody and Flag antibody in mESCs; scale bar, 10 μm. (**G**) Upper panel, representative immunofluorescence images of the anti-Flag antibody and anti-Nucleolin (Ncl) antibody in mESCs. An anti-Flag antibody was used to visualize the Nat10 signal, and DAPI used to visualize the nuclei. Scale bar, 10 μm. Bottom panel, Immunofluorescence images of the Nat10 antibody and Hp1α antibody in mESCs; scale bar, 10 μm. (**H**) Immunofluorescence of the Nat10 in ESCs at interphase or metaphase arrested by nocodazole treatment. Nuclei were visualized with DAPI. Scale bar, 10 μm..

the presence of Dox (1 μg/ml) were called *Nat10* KD mESCs, and the cell lines cultured in the absence of Dox called *Nat10* CON mESCs. While *Nat10* CON mESCs presented a normal morphology, *Nat10* KD mESCs displayed a loss of typical clonal morphology with a flat appearance (Fig. 2A).

To comprehensively assess the alterations in gene expression in mESCs resulting from *Nat10* depletion, we performed mRNA sequencing in *Nat10* KD and *Nat10* CON mESCs with three replicates. Principal component analysis (PCA) revealed obvious distinctions between the expression profiles of *Nat10* KD and *Nat10* CON mESCs (Fig. 2B). Compared with *Nat10* CON, *Nat10* KD resulted in the downregulation of 1,256 genes and the upregulation of 1,650 genes (Fig. 2C). Gene Ontology analysis of biological processes (GO-BP) of the downregulated genes demonstrated that most of the enriched terms were related to pluripotency (Fig. 2D and Supplementary Table S8). Moreover, the transcript levels of most of the pluripotency genes decreased after *Nat10* KD in mESCs (Fig. 2E). We confirmed the expression levels of core pluripotency genes, such as *Oct4*, *Nanog*, and *Esrrb*, after *Nat10* KD via RT−qPCR and Western blot assays. All these factors were downregulated in the *Nat10*-inducible KD mESCs (Fig. 2F, 2G). These data reveal that Nat10 is essential for maintaining the pluripotency of mESCs.

Nat10 represses 2C genes

To further investigate the roles of Nat10 in mESCs, we first used published data to determine the expression of *Nat10* during embryonic development [59]. Consistent with previous observations [60], the expression of *Nat10* was lowest at the two-cell embryonic stage (Supplementary Fig. S3A). Furthermore, when looking into two independent Zscan4-positive and -negative (Zscan4$^+$ vs Zscan4$^-$) mESCs [61, 62], the expression of *Nat10* was slightly lower in Zscan4$^+$ cells than in Zscan4$^-$ cells (Supplementary Fig. S3B). These observations motivated us to explore the relationship between Nat10 and genes specifically expressed in 2-cell embryos, which are also called 2C genes.

Most of the 2C genes, from a published paper [21], were activated in *Nat10*-KD mESCs (Fig. 3A), including *Dux*, *Zscan4*, *Usp17l*, and *Tcstv3* (Fig. 3B; Supplementary Fig. S3C). Moreover, transposons closely related to 2C genes, such as *MERVL_int* and *MT2_Mm*, were also upregulated after *Nat10* KD (Fig. 3C). We next determined the expression levels of the 2C marker *Zscan4* and other 2C genes, such as *Dux* and *Gm12794*, after *Nat10* depletion via RT−qPCR and western blot. All these genes were upregulated in *Nat10* KD mESCs. To better test the proportion of 2CLCs, we performed immunofluorescence by using the Zscan4 protein to identify 2CLCs. Through counting the Zscan4-positive cells, the percentage of 2CLCs was 3.7% in *Nat10* CON and increased to 8.5% after *Nat10* KD (Fig. 3D-F). These results suggest that Nat10 is a suppressor of 2C genes in mESCs.

We then constructed a *3 × Flag-Nat10*-overexpressing (OE) cell line (Fig. 3G). The *Nat10* OE mESCs maintained the same typical undifferentiated clones in morphology as the *Nat10* CON mESCs did (Supplementary Fig. S3D). We examined the expression of Zscan4 and other 2C genes via western blotting and qPCR. In contrast, Zscan4, the typical 2C gene, was reduced at both the protein and mRNA levels after *Nat10* OE in mESCs. Other classical 2C genes were also downregulated, as shown by qPCR (Fig. 3H,I). However, the protein and mRNA levels of Oct4 and Nanog were greater in *Nat10* OE mESCs than in *Nat10* CON mESCs (Fig. 3H,I), in contrast to *Nat10* KD mESCs.

Additionally, we attempted to rescue the changes in the mRNA levels of 2C genes and pluripotency genes by transfecting exogenous *Nat10* in these cells which were already cultured for 48 h in the presence of Dox to induce *Nat10* KD. Like *Nat10* KD mESCs, Nat10 rescue (*Nat10* KD + *Nat10* OE) mESCs still maintained a differentiated morphology (Supplementary Fig. S3D) and could not reverse the phenotype caused by *Nat10* depletion. Consistent with the morphology, exogenous *Nat10* reversed the increase in 2C genes induced by *Nat10* KD, while pluripotency markers such as Oct4 and Nanog could not be rescued (Supplementary Fig. S3E, S3F).

Moreover, we overexpressed WT *Nat10* or *Nat10*^{G641E} mutants prior to Dox-inducible KD. By western blotting, overexpression of WT *Nat10* could partly rescue the protein levels of pluripotency genes and fully rescue protein level of Zscan4, representative of 2C genes, whereas the mutant failed to rescue protein levels of both pluripotency and Zscan4 genes (Supplementary Fig. S4).

Together, these data suggest that Nat10 may play a role in suppressing 2C gene expression in mESCs and maintaining the balance of the 2C state and pluripotency genes in mESCs.

Nat10 KD decreases ac^{4}C mRNA modification in mESCs

Nat10 is the only known acetyltransferase that catalyzes the ac^{4}C modification of RNA [63, 64]. We first used dot blotting to detect the ac^{4}C levels in total RNA. The ac^{4}C levels in total RNA decreased significantly after *Nat10* KD in mESCs (Supplementary Fig. S5A). We further performed acetylated RNA immunoprecipitation followed by sequencing (acRIP-seq) in the *Nat10* CON and *Nat10* KD mESCs and compared the ac^{4}C peaks with those in the *Nat10* CON mESCs to obtain specific downregulated peaks after *Nat10* KD (Fig. 4A). In total, we obtained 2,560 peaks in *Nat10* CON mESCs and 3,765 peaks in *Nat10* KD mESCs, in two replicates. We then defined the peaks that decreased with decreasing mRNA levels under Log_2 (fold change) < -1 and FDR < 0.05 conditions as specific peaks. More specific peaks decreased after *Nat10* KD (Supplementary Fig. S5B). To better understand the similarities or differences between our analysis and a published study (GSE226748), we first analyzed these data and revealed that 3,939 peaks were downregulated after *NAT10* KD in hESCs (Supplementary Fig. S5C and D). By comparing these peaks with those downregulated after *Nat10* KD in mESCs (Supplementary Table S9), we found 958 shared peaks (Supplementary Fig. S5D). Further GO functional enrichment analysis revealed that genes related to mRNA splicing, mRNA metabolism and mechanisms associated with pluripotency-related terms were enriched in the shared peaks (Supplementary Fig. S5E), suggesting that these processes are regulated by ac^{4}C modification and might be conserved between mESCs and hESCs. Additionally, in mESCs, ac^{4}C may be related to chromosome maintenance and epigenetic regulation terms, whereas in hESCs, ac^{4}C was associated with translation and rRNA processing-related terms (Supplementary Fig. S5F and G). When we analyzed the distribution of ac^{4}C on mRNA transcripts after *Nat10* depletion, more than 50% of the ac^{4}C peaks were located in gene

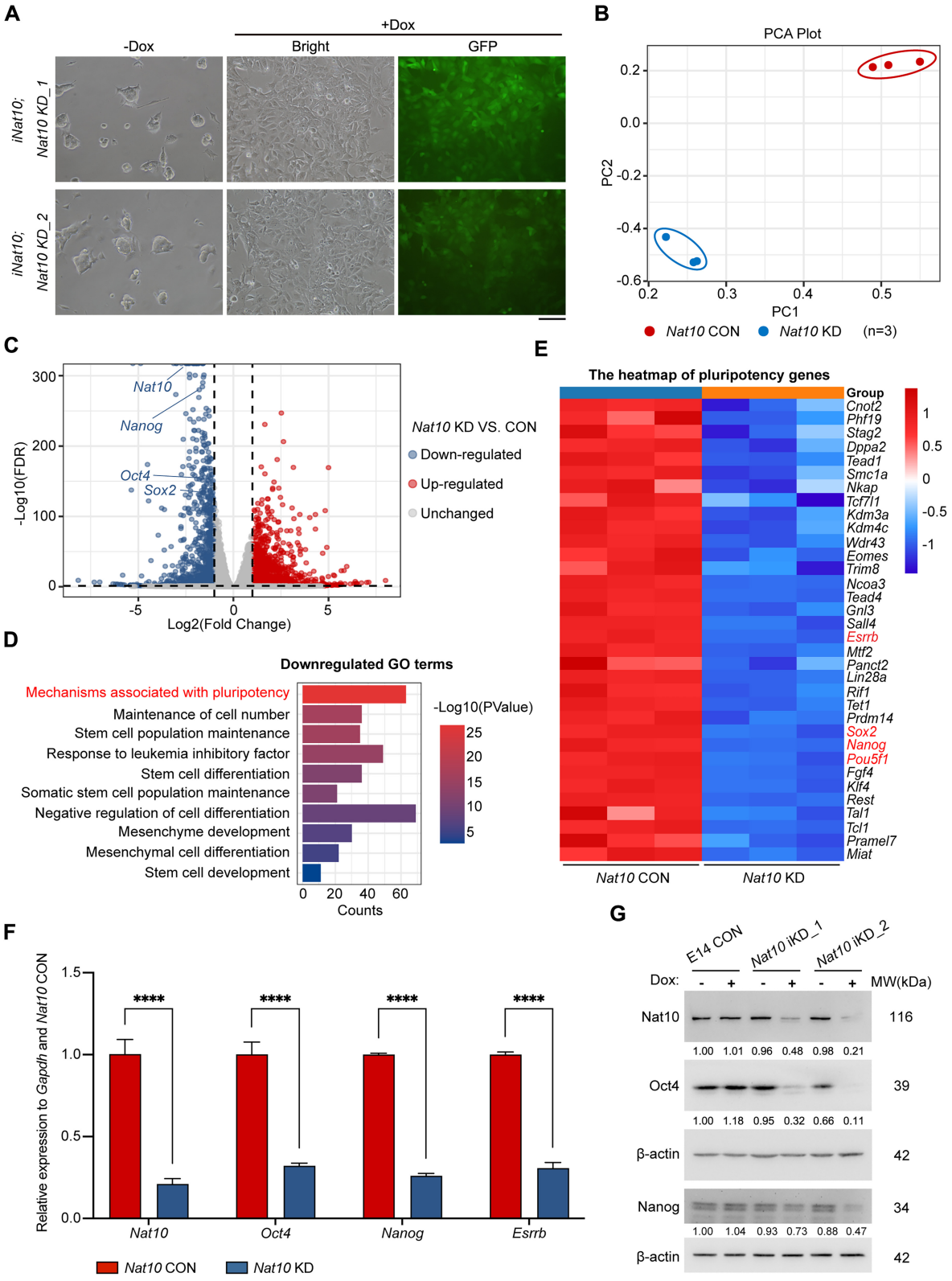

Figure 2. *Nat10* is required for maintaining the expression levels of key pluripotency genes in mESCs. (**A**) Representative images of the morphology of *Nat10* control (without Dox treatment, -Dox) versus *Nat10* KD cells (with Dox treatment for 48 h, +Dox) under fluorescence and bright-field microscopes; KD_1 and KD_2 indicate two independently induced *Nat10* KD cell lines. Scale bar, 100 μm. (**B**) Principal component analysis (PCA) plot depicting the clustering of the *Nat10*-KD group versus the *Nat10*-CON group. Each symbol represents an RNA-seq sample. (**C**) Volcano plots showing differentially expressed genes in *Nat10*-KD mESCs compared with CON mESCs ($n = 3$). Represent genes upregulated and downregulated by *Nat10*-KD were highlighted in color. The false discovery rate (FDR) was <0.05, and the Log2-fold change (FC) was >1 or <-1. (**D**) The enriched Gene Ontology (GO) terms of downregulated differentially expressed genes (DEGs) in *Nat10* KD compared with *Nat10* CON mESCs. (**E**) Heatmap showing downregulated pluripotent gene expression from RNA-seq analysis in *Nat10*-KD and CON mESCs. (**F**) Quantitative RT–PCR (qPCR) of the expression of the pluripotent genes *Oct4*, *Nanog* and *Esrrb* normalized to *Gapdh*. The data are presented as the means ± SEMs, $n = 3$. **** $P < 0.0001$. (**G**) Representative western blot analysis of Oct4, Nanog and Nat10 expression. β-actin served as the loading control. The data are representative of three independent experiments.

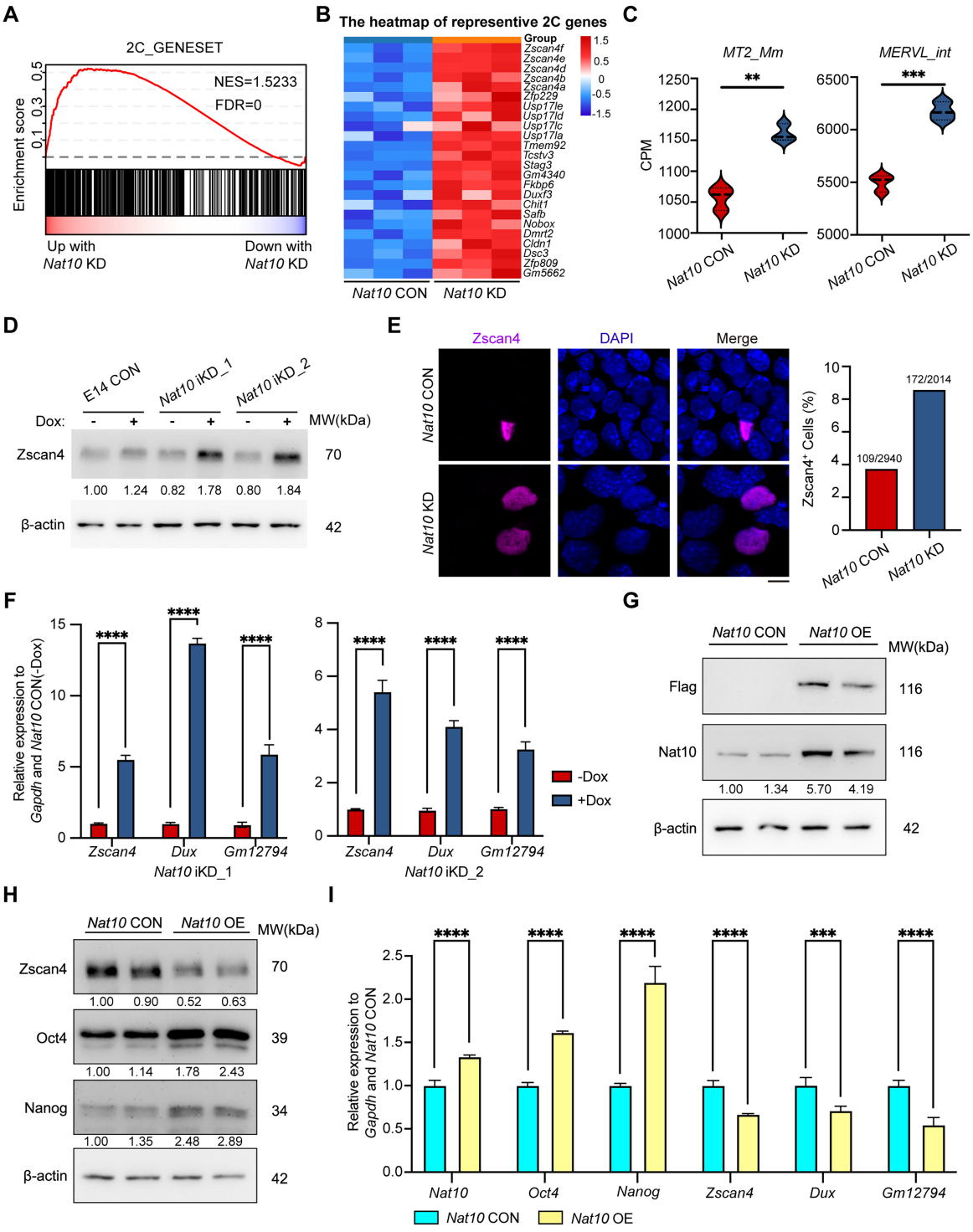

Figure 3. Nat10 represses 2C genes. (**A**) Gene set enrichment analysis (GSEA) using the 2-cell signature genes defined in Macfarlan *et al.* [21] (GSE33923) to compare *Nat10*-KD with CON mESCs. NES, normalized enrichment score. Three biological replicates were used for each RNA-sequencing sample. (**B**) Heatmap showing the upregulated 2C genes from RNA-Seq analysis in *Nat10*-KD and CON mESCs. (**C**) Violin plot showing the expression of the 2-cell-related transposable elements (TEs) *MERVL_int* and *MT2_Mm*. The gene expression level was quantified as counts per million (CPM). ** $P < 0.01$, *** $P < 0.001$ (two-tailed unpaired *t* test). (**D**) Representative western blot analysis of Zscan4 expression in two inducible *Nat10*-KD mESC lines. β-actin served as the loading control. (**E**) Immunofluorescence of Zscan4 in *Nat10* CON and *Nat10* KD mESCs. Left panel, representative images of Zscan4 protein immunofluorescence. Scale bar, 10 μm. Right panel, proportion of Zscan4-positive (Zscan4$^+$) cells based on immunofluorescence images. The number of cells counted is shown at the top of the bar. (**F**) Quantitative RT–PCR (qPCR) of the expression of the 2C marker genes *Zscan4, Dux* and *Gm12794* in two *Nat10* inducible KD cell lines normalized to *Gapdh*. The data are presented as the means ± SEMs, $n = 3$. **** $P < 0.0001$. (**G**) Representative western blot analysis of the expression of Nat10 and Flag in *Nat10* CON and *Nat10*-overexpressing (*Nat10* OE) mESCs. β-Actin served as the loading control. (**H**) Representative western blot analysis of the expression of Nanog, Oct4 and Zscan4 in *Nat10* CON and *Nat10* OE mESCs. β-Actin served as the loading control. (**I**) Quantitative RT–PCR (qPCR) of the transcription levels of the *Nat10*, *Oct4*, *Nanog* and 2C genes *Zscan4, Dux and Gm12794* normalized to *Gapdh*. The data are presented as the means ± SEMs, $n = 3$. *** $P < 0.001$, **** $P < 0.0001$. (**D-I**), experiments were conducted at least three times with similar results.

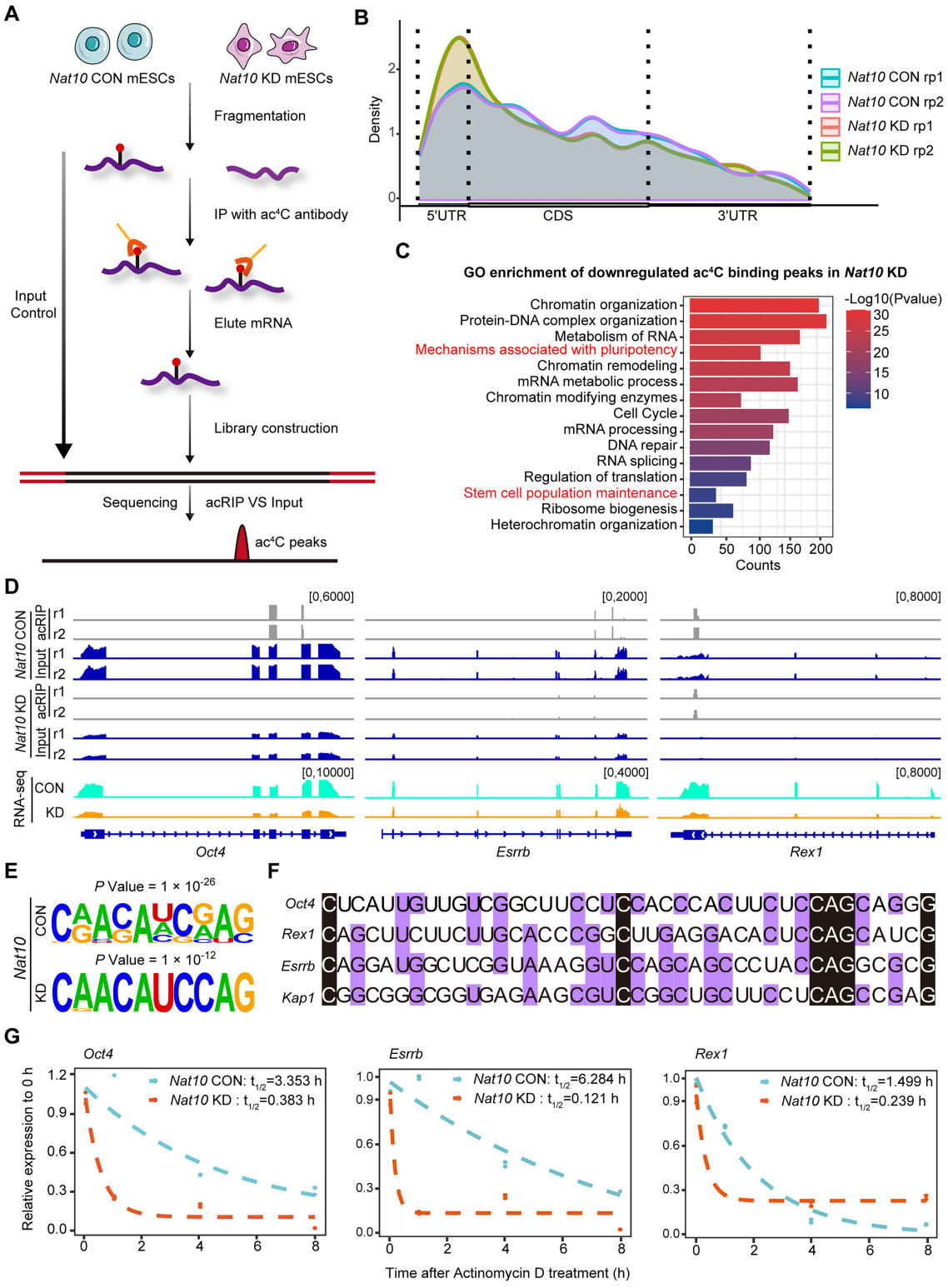

Figure 4. The Nat10-catalyzed ac^{4}C modification affects the transcriptome of pluripotency and chromatin remodeling genes in mESCs. (**A**) Schematic of acRIP-seq. The RNA was first extracted from the *Nat10* CON and *Nat10* KD mESCs, and then the RNA was randomly fragmented to approximately 200 nt by RNA fragmentation reagents. The anti-ac^{4}C antibody was coupled with beads. The RNA fragments were incubated with bead-linked antibodies, and the captured RNA was subsequently eluted from the complexes and purified. The RNA libraries for the IP and input samples were then sequenced. (**B**) Distributions of the ac^{4}C peaks across transcripts. The distributions of ac^{4}C peaks along the 5′UTR, CDS and 3′UTR of mRNAs in two biological replicates of the *Nat10* CON and *Nat10* KD samples are shown. (**C**) GO functional enrichment analysis of genes marked by genes with downregulated ac^{4}C peaks in *Nat10*-KD mESCs compared with *Nat10*-CON mESCs. (**D**) IGV tracks displaying the RNA-seq and acRIP-seq signals across target transcripts of *Oct4*, *Esrrb* and *Rex1*. (**E**) Most significant motif in the *Nat10* CON and *Nat10* KD mESC peaks. (**F**) The CAG motif is conserved among the mouse *Oct4*, *Esrrb*, *Rex1*, and *Kap1* transcripts. The specific sequences of these transcripts were predicted via acRIP-seq analysis and obtained from the National Center for Biotechnology Information-National Institutes of Health (NCBI-NIH) database. (**G**) RT–qPCR analysis comparing the mRNA decay rates of *Oct4*, *Esrrb* and *Rex1* in *Nat10* CON and *Nat10* KD mESCs. The experiments were conducted at least three times with similar results.

coding regions. The distribution of the peaks across transcripts revealed a shift in enrichment from gene coding regions in the vicinity to 5′ untranslated regions (5′ UTRs) (Fig. 4B; Supplementary Fig. S5H).

Functional enrichment analysis of the genes with downregulated peaks showed significant enrichment in terms related to pluripotency and chromatin organization (Fig. 4C). Notably, the genes with downregulated ac^{4}C peaks were related to heterochromatin modifiers such as *Chaf1a*, *Rif1*, *Atrx* and *Hp1α*, which represses 2C genes [18], as well as *Kap1*. The ac^{4}C modifications also were present on the mRNAs of pluripotency factors such as *Oct4*, *Esrrb* and *Zfp42* (also known as *Rex1*), which are considered important naïve state marker genes in mESCs [65, 66] and were significantly reduced after *Nat10* KD (Fig. 4D). However, ac^{4}C modifications were minimal on the mRNAs of the 2C genes (Supplementary Fig. S5I).

Consistent with previous study [67], "CXXCXXCXX" was the most enriched motif at the ac^{4}C peak (Fig. 4E). Our acRIP-seq data revealed that the transcripts of the pluripotency genes shown above and the heterochromatin organization-related gene *Kap1* could be acetylated at cytosine. We aligned the four sequences and showed that they had a high degree of consistency, with these sequences enriching at least three "CXX" repeats on their transcripts and sharing the common sequence "CAG" (Fig. 4F). These data may explain why ac^{4}C modifications preferentially occur on these genes.

It has been reported that ac^{4}C modification can promote mRNA stability [1]. We performed an RNA stability assay and validated that the stability of *Oct4*, *Esrrb* and *Rex1* mRNAs dramatically decreased after *Nat10* KD in mESCs (Fig. 4G).

We also used Remodelin, a specific inhibitor of NAT10 that can inhibit acetyltransferase activity [68], to examine the inhibitory effects of Nat10. The mRNA levels of pluripotency genes were also lower after 20 μM Remodelin treatment for three passages than those after DMSO treatment, which served as a vehicle control (Supplementary Fig. S5J). In addition, the expression of key 2C genes, such as *Zscan4, Dux, Gm12794, Tcstv1/3*, and *Tbx3,* the upstream of *Zscan4* [69], was increased by qPCR compared with that of the DMSO control (Supplementary Fig. S5J). These data were consistent with those from *Nat10* KD experiments, confirming that N^4-acetylcytidine (ac^{4}C) writer activity is important for maintaining the mRNA levels of pluripotency genes and of heterochromatin remodelers in suppressing 2C genes.

The above data indicate that the mRNAs of core pluripotency genes can be modified by ac^{4}C, which results in increased stability of mRNAs encoding pluripotency factors, whereas the 2C gene levels are unlikely to be directly impacted by ac^{4}C modification of their mRNAs.

Nat10 targets and promotes the stability of *Kap1* mRNA

Since 2C genes are not directly regulated by the ac^{4}C modification of mRNAs, we explored how Nat10 regulates the expression levels of 2C genes. After *Nat10* KD, the peaks downregulated by ac^{4}C were also significantly enriched in chromatin organization (Fig. 4C). As many heterochromatin-associated factors can regulate the expression of 2C genes, Nat10 may indirectly regulate the expression levels of 2C genes through chromatin modification. There were 164 downregulated genes likely regulated by ac^{4}C modification according to the analysis of the acRIP-seq data and RNA-seq data (Fig. 5A). Among 164 genes, 25 genes were enriched in the chromatin organization term (Fig. 5B), including the mRNA encoding Kap1, which is a heterochromatin-binding protein to H3K9me3 (Fig. 5C and D). To investigate whether this mechanism in mESCs is specific, we further analyzed the acRIP-Seq data from hESCs (GSE226748) and used IGV to display the acRIP-Seq signals for the target transcripts of *KAP1* and *OCT4*. In *NAT10*-deficient hESCs, ac^{4}C signaling on *OCT4* mRNA was notably decreased, similar to that in mESCs, whereas modifications on *KAP1* mRNA were not changed (Supplementary Fig. S6A). Additionally, the transcription level of *KAP1* was unchanged in *NAT10* KD hESCs, compared with that in KD controls (Supplementary Fig. S6B). The above data suggest that Nat10-mediated ac^{4}C modification might target *Kap1* mRNA only in mESCs, unlike in hESCs. Indeed, Kap1 was significantly decreased at the transcript and protein levels in the *Nat10*-KD mESCs, whereas another key H3K9me3 reader protein, Hp1α, changed slightly after *Nat10* depletion (Fig. 5E and F). Kap1 is involved in heterochromatin maintenance and the inhibition of 2C genes in mESCs [17, 70, 71]. We compared the interactions of Kap1 with the histone modification H3K9me3 in *Nat10* CON and *Nat10* KD mESCs. Kap1 pulled down a lower amount of H3K9me3 in *Nat10* KD mESCs (Fig. 5G). Moreover, the level of the histone modification H3K9me3 was also reduced after *Nat10* depletion (Fig. 5H). Reduced H3K9me3 and Kap1 may decrease the H3K9me3 heterochromatin complex in *Nat10*-depleted mESCs. Moreover, H3K9me3 chromatin immunoprecipitation sequencing (ChIP-seq) revealed that H3K9me3 was reduced among the 2,214 downregulated peaks in *Nat10* KD mESCs compared with *Nat10* CON mESCs (Fig. 5I and Supplementary Table S10). By focusing on the upregulated 2C genes in our RNA-seq data, we found that H3K9me3 at these genes was indeed decreased after *Nat10* KD (Fig. 5J; Supplementary Fig. S6C). By ChIP–qPCR analysis, enrichment of H3K9me3 at the *Zscan4* promoter was decreased after *Nat10* KD (Fig. 5K). In contrast, overexpression of *Kap1* in *Nat10*-KD mESCs reversed the increased expression levels of 2C genes in *Nat10*-KD cells (Supplementary Fig. S6D and E).

Next, we explored how Nat10 regulates Kap1 expression levels. Given that *Kap1* mRNA can be modified directly by ac^{4}C (Fig. 5C), we examined the mRNA stability of *Kap1*. The stability of *Kap1* mRNA decreased after *Nat10* KD in mESCs (Fig. 5L). To address whether the Nat10 acetyltransferase domain has functions other than acting as an ac^{4}C writer, we detected the common acetylation histone modifications, such as H3K27ac and H3K9ac, in *Nat10* inducible KD mESCs. The two modifications were nearly unchanged after *Nat10* KD, which is also consistent with the work published recently [37] (Supplementary Fig. S6F). We also performed RNA polymerase II ChIP-qPCR. The enrichment of RNA Pol II at the *Kap1* promoter was nearly unchanged after *Nat10* KD (Supplementary Fig. S6G), suggesting that Nat10 promotes the mRNA levels of *Kap1* in mESCs, unlikely by mediating histone acetylation or by transcription of *Kap1* mRNA.

To further explore whether Nat10 catalytic activity is essential for *Kap1* and 2C gene-related mRNAs, we generated a catalytically dead G641E mutant of Nat10 (Nat10^{G641E}) following previous methods [37] (Fig. 6A). We overexpressed full-length *Nat10* (*Nat10* FL) or *Nat10*^{G641E} in WT mESCs and detected the Nat10 expression level and global ac^{4}C modification level in total RNA via western blot and dot blot assays.

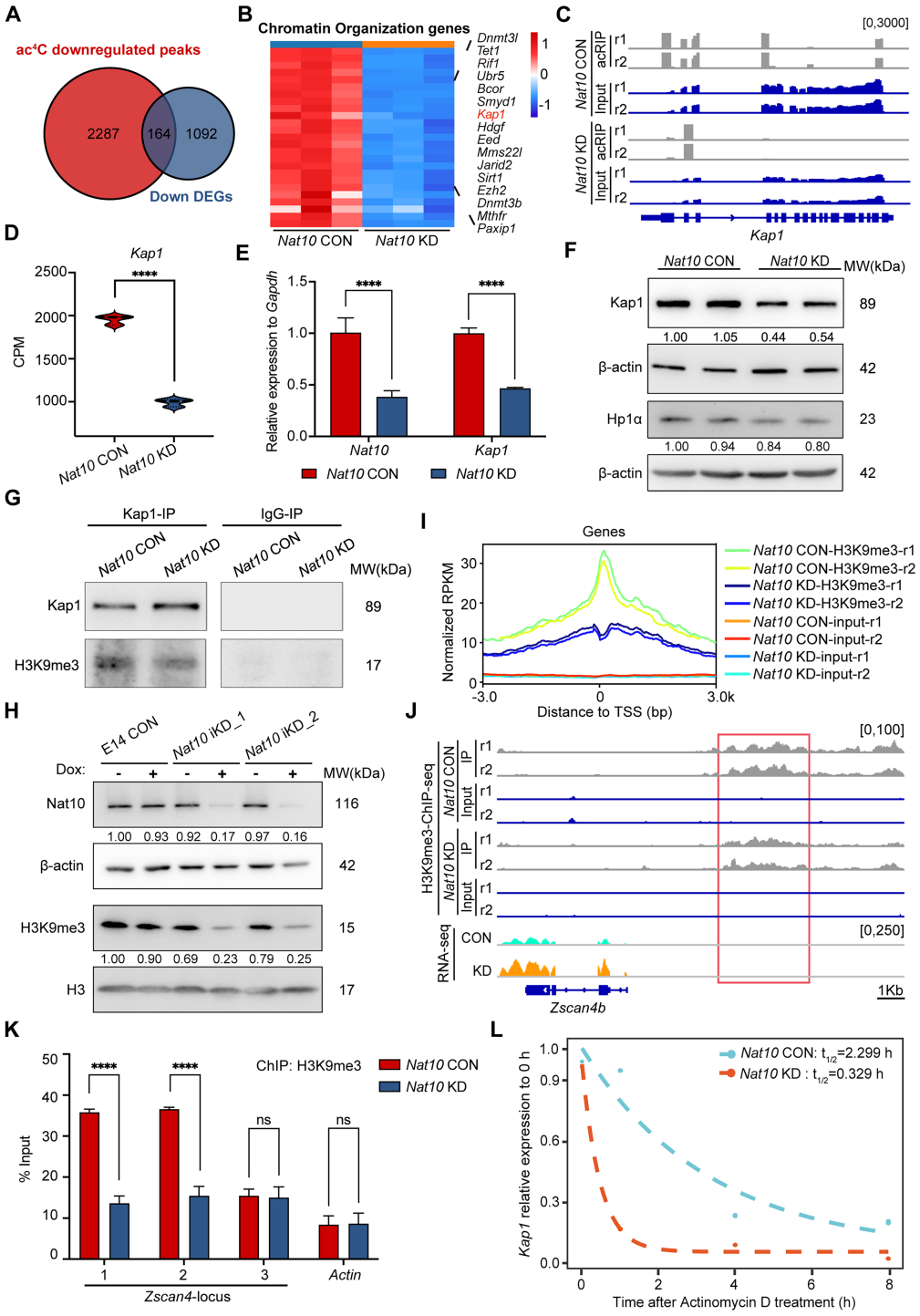

Figure 5. Nat10 targets and promotes the stability of *Kap1* mRNA. (**A**) Venn diagram showing overlapping genes between downregulated ac^{4}C peaks in *Nat10* KD mESCs (left circle) and downregulated DEGs in *Nat10* KD mESCs (right circle). (**B**) Heatmap showing the downregulated genes from RNA-Seq analysis in *Nat10*-KD and CON mESCs associated with chromatin organization. (**C**) IGV tracks displaying the acRIP-seq signal across target transcripts of *Kap1*. (**D**) Violin plot showing the expression of *Kap1* in *Nat10* CON and *Nat10* KD mESCs. The gene expression level was quantified as counts per million (CPM). $^{****}P < 0.0001$ (two-tailed unpaired *t* test). (**E**) Quantitative RT–PCR (qPCR) of the transcription levels of *Nat10* and *Kap1* normalized to *Gapdh*. The data are presented as the means ± SEMs, $n = 3$. $^{****}P < 0.0001$. (**F**) Representative western blot analysis of the expression of Kap1 and Hp1α. β-Actin served as the loading control. (**G**) The IP-western approach demonstrated the critical role of Nat10 in maintaining the interaction between Kap1 and H3K9me3. (**H**) Representative western blot analysis of the expression of Nat10 and H3K9me3 histone modifications in two inducible *Nat10*-KD cell lines. H3 and β-actin served as loading controls. (**I**) H3K9me3 binding to the TSS region among the downregulated peaks in *Nat10* CON and KD mESCs, data were normalized by reads per kilobase per million mapped reads (RPKM). (**J**) IGV tracks displaying the RNA-seq and ChIP-seq signals across H3K9me3 binding sites on *Zscan4b*. Three biological replicates are overlaid in the RNA-seq panel. (**K**) ChIP–qPCR analysis of H3K9me3 enrichment at proximal regions of the *Zscan4* promoter. The *β-actin* locus served as a negative control. Mean ± SEM from three replicates, $^{****}P < 0.0001$, and ns, no significant difference. (**L**) RT–qPCR analysis comparing the mRNA decay rate of *Kap1* in *Nat10* CON and *Nat10* KD mESCs. The experiments were conducted at least three times with similar results. (**E**), (**F**), (**G**), (**H**), (**K**), and (**L**) experiments were conducted at least three times, each yielding similar results.

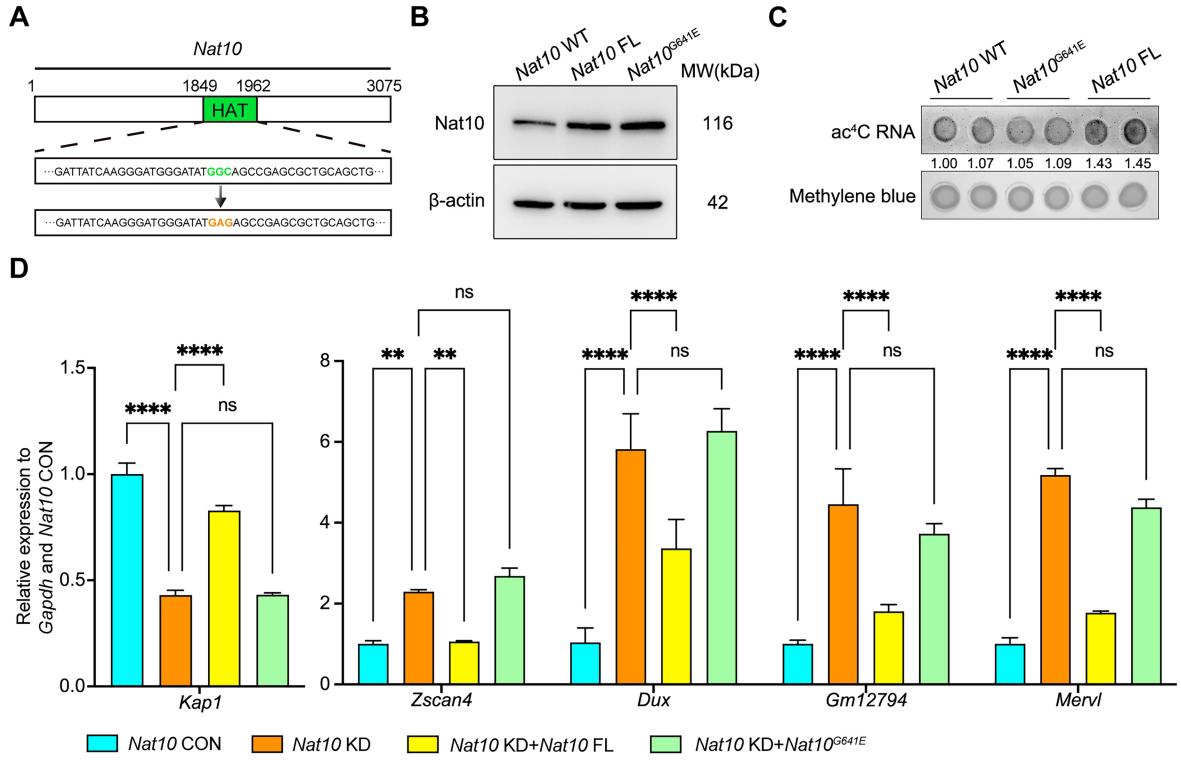

Figure 6. The impact of Nat10 catalytic activity on *Kap1* and 2C genes. (**A**) Schematic of the Nat10^{G641E} mutant construction. (**B**) Representative western blot analysis of Nat10 expression in *Nat10* WT, *Nat10* FL-overexpressing and *Nat10*^{G641E}-overexpressing mESCs. β-Actin served as the loading control. (**C**) Representative dot blot of ac^{4}C modification in total RNA from *Nat10* WT, *Nat10*^{G641E}-overexpressing and *Nat10* FL-overexpressing mESCs. Methylene blue staining was used as the control. The signal intensity below the gel was quantified relative to that of the corresponding Methylene blue. (**D**) Quantitative RT–PCR (qPCR) of the mRNA levels of the *Kap1* and 2C genes *Zscan4, Dux, Gm12794*, and *Mervl* in *Nat10* CON, *Nat10* KD, *Nat10* KD + *Nat10* FL OE and *Nat10* KD + *Nat10*^{G641E} OE mESCs. *Nat10* KD + *Nat10* FL OE refers to the overexpression of the full-length *Nat10* in *Nat10* KD mESCs, and *Nat10* KD + *Nat10*^{G641E} OE refers to the overexpression of the *Nat10*^{G641E} mutant in *Nat10* KD mESCs, normalized to *Gapdh*. The data are presented as the means ± SEMs, $n = 3$. $^{**}P < 0.01$, $^{****}P < 0.0001$, and ns, no significant difference.

Unlike the full-length *Nat10* (*Nat10* FL), the *Nat10*^{G641E} mutant was unable to efficiently catalyze RNA acetylation (Fig. 6B,C), indicating successful construction of a catalytic mutant of Nat10. We transiently overexpressed *Nat10* FL and the *Nat10*^{G641E} mutant in *Nat10* KD mESCs for 48 h. We detected the *Kap1* mRNA acetylation level via acRIP-qPCR, and used the sequence identified by acRIP-Seq and predicted by PACES [67] to design specific primers (Supplementary Fig. S6H and Supplementary Table S3). The ac^{4}C enrichment on *Kap1* mRNA was decreased after *Nat10* KD and could be partly rescued by overexpression of *Nat10* FL (full-length) but not by overexpression of *Nat10*^{G641E} mutant (Supplementary Fig. S6I). Additionally, the mRNA level of *Kap1* was rescued after *Nat10* FL overexpression, whereas *Nat10*^{G641E} mutant overexpression failed to increase *Kap1* mRNA levels. Coincidentally, the upregulation of 2C-genes caused by *Nat10* KD can be repressed by *Nat10* FL but not by the *Nat10*^{G641E} mutant (Fig. 6D). Hence, the catalytic activity of Nat10 is important for repressing the 2C genes via promoting *Kap1*.

Together, Nat10 maintains the mRNA level of *Kap1* by modulating its mRNA stability via acetylation. A reduction in Kap1 could be one of the major factors responsible for the increased expression of 2C-genes in *Nat10* KD mESCs.

Nucleolar/ribosomal functions of Nat10

Nat10 is known to serve as a nucleolar-associated protein [57], and most of its interacting proteins are related to ribosome biogenesis (Fig. 1E). We detected the expression of the rRNA components 18S rRNA, 28S rRNA and pre-rRNA in *Nat10* CON and *Nat10* KD mESCs via qPCR. *Nat10* KD had little effect on 18S rRNA transcripts but increased 28S rRNA transcripts and decreased pre-rRNA transcripts (Fig. 7A). Although 28S rRNA was slightly increased, previous work has shown that mature 18S, 5.8S, and 28S rRNAs are processed by removing the 5′-ETS/3′-ETS surrounding the pre-rRNA and the intermediate ITS1/ITS2 fragments [72], which might imply that pre-rRNA may play more important roles in rRNA synthesis and processing. When we analyzed our RNA-seq data via gene set enrichment analysis (GSEA), we noticed that most rRNA processing-related genes were downregulated in *Nat10* KD mESCs (Fig. 7B), suggesting that rRNA synthesis could be impaired after *Nat10* depletion. Moreover, most ribosome biogenesis-related genes, including *Ncl* and *Npm1*, were downregulated in *Nat10* KD mESCs (Fig. 7C,D). Ncl protein levels were also decreased after *Nat10*-KD (Fig. 7E). To investigate whether reduced Ncl has an effect on the structure of the nucleolus, we performed immunofluorescence microscopy of Ncl in *Nat10* KD mESCs compared with *Nat10* CON mESCs. The number of foci of DAPI-stained heterochromatic regions was reduced after *Nat10* KD. Additionally, high-resolution structured illumination microscopy (SIM) was used and revealed that *Nat10* KD led to the disappearance of the Ncl-marked “ring” structure, which represents the characteristic nucleolar structure of the dense fibrillar component (DFC) region (Fig. 7F,G). Moreover, the number of nucleoli

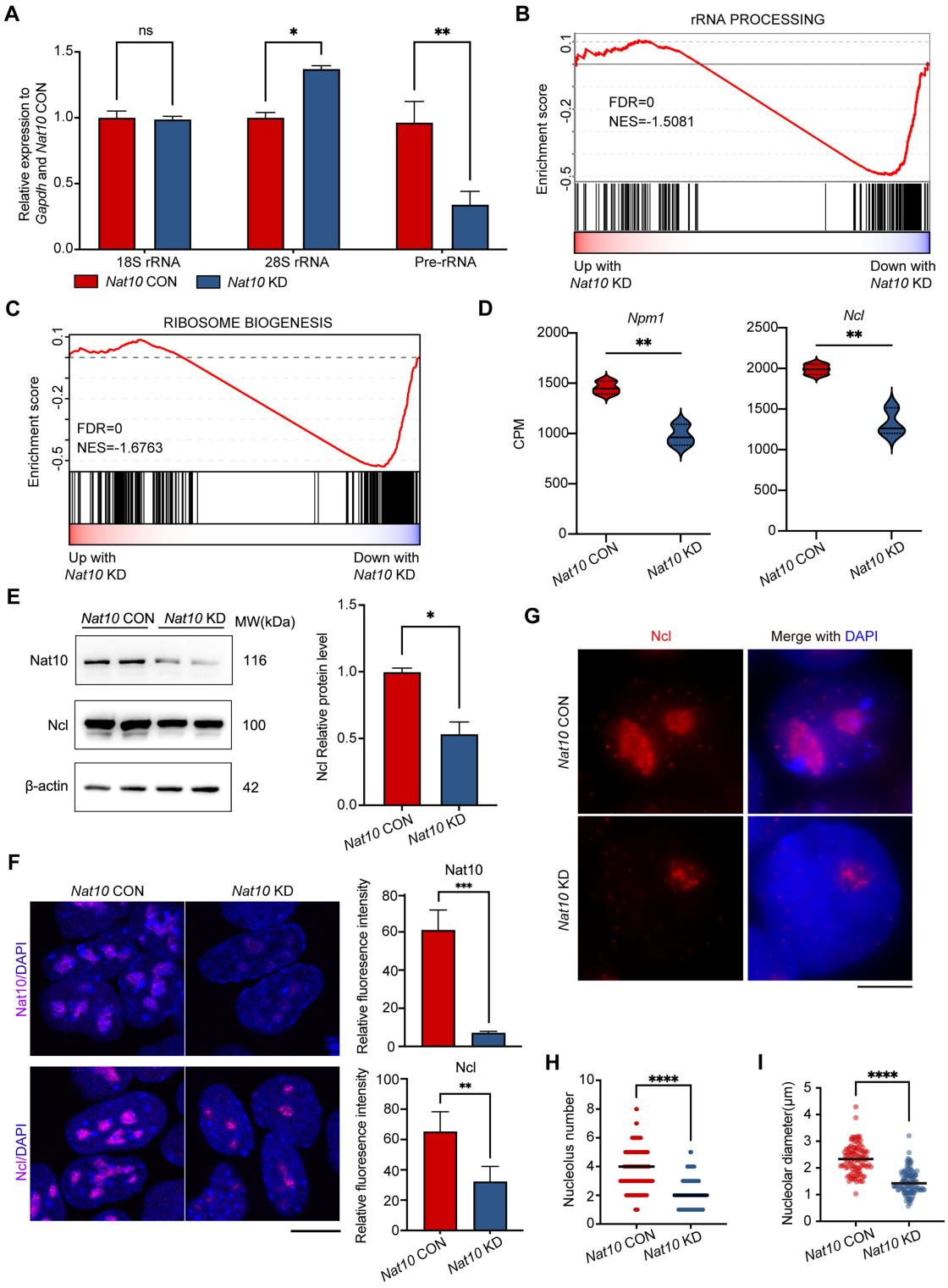

Figure 7. *Nat10* depletion changes ribosome biogenesis. (**A**) Abundance of pre, 18S and 28S rRNAs determined by qPCR normalized to *Gapdh*. The data are presented as the means ± SEMs, $n = 3$. $^{*}P < 0.05$, $^{**}P < 0.01$, and ns, no significant difference. (**B-C**) Gene set enrichment analysis (GSEA) indicating that downregulated genes are highly enriched in the rRNA processing gene set (**B**) and ribosome biogenesis gene set (**C**). NES, normalized enrichment score. Three biological replicates were used for each RNA-seq sample. (**D**) Violin plot showing the expression of the ribosome biogenesis-related genes *Ncl* and *Npm1*. The gene expression level was quantified as counts per million (CPM). $^{**}P < 0.01$ (two-tailed unpaired *t* test). (**E**) Left panel, representative western blot analysis of the expression of Nat10 and Ncl. β-Actin served as the loading control. Right panel, quantification of the grayscale of Ncl. The data are presented as the means ± SEMs, $n = 2$. $^{*}P < 0.05$. (**F**) Immunofluorescence analysis of Nat10 and Ncl. Scale bar, 10 μm. Right panel, quantification of the mean fluorescence intensity of Nat10 and Ncl, $n = 3$ for each *Nat10* CON and *Nat10* KD clone. The data are presented as the means ± SEMs. $^{**}P < 0.01$, and $^{***}P < 0.001$. (**G**) Structured illumination microscopy (SIM) of Ncl. Scale bar, 5 μm. (**H-I**) Quantification of the nucleolar number (**H**) and nucleolar diameter (**I**). The nucleoli were labeled with Ncl and counted manually. More than 100 cells and nucleoles were used for quantification in each group. The data are presented as the means ± SEMs. $^{****}P < 0.0001$. (**A**), (**E**), and (**F**), experiments were conducted at least three times, and similar results were obtained.

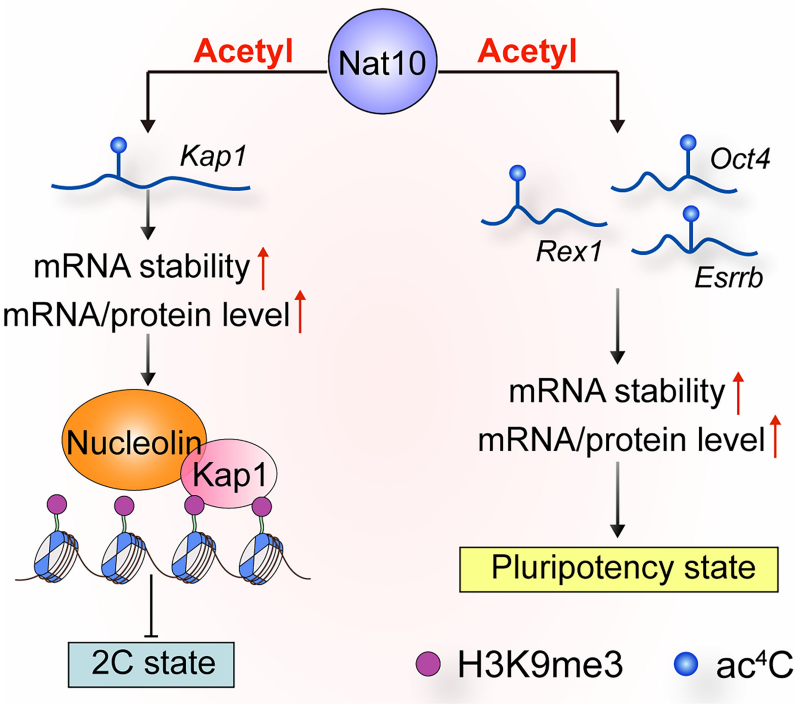

Figure 8. Working model of the role of Nat10-mediated ac^{4}C mRNA modification in regulating the homeostasis of pluripotent and 2C-like states in mESCs. The mRNAs encoding the core pluripotency regulator *Oct4* and other pluripotency genes, *Esrrb* and *Rex1,* can be modified by ac^{4}C acetylation to promote a pluripotent state in mESCs. Heterochromatin *Kap1* can also be acetylated by ac^{4}C modification to promote the stability of *Kap1* mRNA, in turn increasing the abundance of the H3K9me3 complex at 2C genes and subsequently repressing the 2C-like state.

and their sizes were noticeably decreased in *Nat10* KD mESCs (Fig. 7H,I). These data indicate that *Nat10* depletion alters ribosome biogenesis and nucleolar structure.

LINE1 can recruit Ncl and Kap1, and the LINE1-Ncl-Kap1 complex could repress the 2C program and promotes rRNA synthesis in mESCs [73]. As Nat10 could interact with Ncl (Supplementary Fig. S1D) and the protein level of Ncl and Kap1 were both decreased after *Nat10* depletion (Figs 5F and 7E), we then asked how Nat10 functions in the LINE1-Ncl-Kap1 complex. We found ac^{4}C modification was minimal on most *LINE1* elements in *Nat10* CON or *Nat10* KD mESCs (Supplementary Fig. S7A and B). We assessed the expression of transposable elements (TEs) in *Nat10* CON and *Nat10* KD mESCs by analyzing the RNA-seq data. Only a few TEs changed, and almost none of the *LINE1* elements showed changes in expression level after *Nat10* KD (Supplementary Fig. S7C). Next, we used published *LINE1*-ChIRP-seq data [74] to determine whether *LINE1* transcripts can directly target *Nat10*. No *LINE1* enrichment was observed at the *Nat10* locus, whereas obvious enrichment was observed at the *Hdac4* locus, a known *LINE1* target (Supplementary Fig. S7D). We also analyzed the transcriptional level of *Nat10* in *LINE1*-KD mESCs [73]. The transcriptional level of *Nat10* showed minimal change after *LINE1* KD (Supplementary Fig. S7E). These data suggest that Nat10 and LINE1 are unlikely to directly regulate each other.

We hypothesized that Nat10 can bridge the interaction of Ncl and Kap1. We used IP/western approaches to investigate the interactions between Ncl and Kap1 in *Nat10* CON and *Nat10* KD mESCs. Compared with the control, Ncl pulled down a lower amount of Kap1, and Kap1 also pulled down a lower amount of Ncl in *Nat10* KD mESCs (Supplementary Fig. S7F). These findings suggest that *Nat10* depletion can reduce Ncl and Kap1 levels, which can potentially weaken their interactions. This interaction might also regulate 2C-genes in mESCs, providing another perspective on how Nat10 regulates 2C-genes in mESCs for future studies.

Discussion

Epigenetic regulation of heterochromatin is very important for determining the fate of mESCs. Recently, RNA epitranscriptomic modifications, such as N^6-methyladenosine (m^{6}A) modification, have been implicated in regulating the fate of mESCs. Nuclear m^{6}A readers or writers function in maintaining self-renewal or repressing the 2C-like transcriptional program in mouse ESCs [34, 75, 76]. We demonstrated that Nat10-mediated RNA modifications via ac^{4}C acetylation play dual roles in pluripotent and 2C-like states in mESCs.

Fluorescence microscopy experiments revealed strong overlap in the subcellular localization of Nat10 and Ncl, whereas Nat10 and Hp1α seemed to localize only in close proximity but not colocalize. Furthermore, Flag-Nat10 IP-MS revealed that core components of heterochromatin, such as Hp1 proteins or other chromodomain proteins, are not major interactors of Nat10, in contrast to ribosome biogenesis, translation and splicing factors (Fig. 1E and Supplementary Table S7), indicating that Nat10 is a nucleolar protein and may indirectly interact with heterochromatin through Ncl. Nat10 may regulate heterochromatin organization owing to its localization to the nucleolus and implication in rDNA biogenesis rather than a direct connection with perinucleolar heterochromatin itself.

Recently, the modification of ac^4C mRNA mediated by NAT10 is required for the maintenance of self-renewal in hESCs [13]. However, *NAT10* KD in hESCs did not affect the expression levels of typical pluripotency markers, including OCT4, NANOG, and SOX2 [14]. Conventional hESCs are generally considered primed-state PSCs, and mESCs are considered naïve-state PSCs [77–79]. We demonstrated that Nat10 directly regulates the mRNA stability of pluripotency factors via RNA modification in mESCs and suppresses the emergence of a 2C-like state, which is specifically found in mESCs.

Mechanically, Nat10-mediated ac^4C modification can form on the heterochromatin modifier *Kap1* mRNA, repressing the expression of 2C genes in mESCs by affecting H3K9me3 heterochromatin modification (simplified model shown in Fig. 8). Kap1 is known as a 2C transcriptome repressor that directly regulates the expression of *Dux* via Dcaf11-mediated Kap1 degradation [17, 28, 44]. Our data demonstrate that Nat10-mediated ac^4C can be a new upstream regulator of Kap1 in the repression of 2C genes. Meanwhile, we also analyzed the *KAP1* mRNA in hESCs by public data and showed no regulation by NAT10, indicating that the mechanism described in this work is specific to mESCs, which might contribute to understand the zygotic genome activation (ZGA) process during mouse embryos development. The limitation of this work is that only acRIP-seq is used to study the *Kap1* mRNA acetylation level. Future studies will be needed to validate the specific acetylation sites of mature *Kap1* mRNAs. Recently, Nat10 has also been shown to regulate R-loops at specific genes in a NAT10 catalytic activity dependent manner [80]. As the level of transcription initiation of *Kap1* was not changed (Supplementary Fig. S6G), the effect of *Nat10* KD on the *Kap1* mRNA could also be owing to an absence of R-loop resolution.

2CLCs [21] can be good models for studying the transition between totipotency and pluripotency *in vitro*, and are important for the formation of totipotent stem cells [81], like zygotes and 2-cell-stage embryos [82]. Epigenetic regulation by small molecules such as crotonic acid, DOT1L (DOT1-like histone lysine methyltransferase that methylates H3K79) inhibitor or the spliceosome inhibitor PlaB can facilitate the expression of 2C genes and reprogram pluripotent mouse ESCs to a totipotent state [56, 83, 84]. We showed that the inhibition of Nat10 by Remodelin can also promote the expression of 2C genes. Hence, Nat10 is a novel repressor of 2C genes, and treatment with Remodelin might be a new approach to obtain 2CLCs in combination with known chemicals.

Taken together, our data identify a novel role for Nat10 in regulating 2C genes and thus balancing the pluripotent and 2C-like states in mESCs via ac^4C modification of mRNAs. The stabilization of *Kap1* mRNAs promoted by Nat10-mediated ac^4C acetylation and the interaction with Ncl could be a major mechanism by which 2C genes are suppressed.

Acknowledgements

We thank Jiao Yang for assisting in the construction of the 3 × Flag-Kap1 overexpression plasmid.

Author contributions: G.F. performed most of the experiments and prepared the manuscript. G.Y. performed the bioinformatic analyses and revised the manuscript. Y.L., Y. Yue, X.G., and J.W. constructed the *Nat10* inducible knockdown cell line. C.L. and J. Li assisted with western blot and ChIP assays of ESCs and revised the manuscript. J.Lu assisted with the immunofluorescence microscopy. Y. Yu, Z.J., and Y.W. conducted some of the experiments and discussed the experiments and data analysis. F.L. provided the E14 *Nat10* inducible knockdown mESCs, advised the project, and revised the manuscript. L.L. conceived the project, designed the experiments, and revised the manuscript.

Supplementary data

Supplementary data is available at NAR online.

Conflict of interest

The authors declare that they have no competing interests.

Funding

This work was supported by the National Natural Science Foundation of China (32030033, 82230052, 322611605). Funding to pay the Open Access publication charges for this article was provided by the National Natural Science Foundation of China.

Data availability

All the data are available in the main text or the supplementary materials. The *LINE1*-ChIRP-seq data for mESCs were downloaded from published data (GSE125766), and the RNA-seq data for *LINE1* CON and KD in mESCs were downloaded from published data (GSE100939). The raw RNA-seq, H3K9me3-ChIP-seq and acRIP-seq data generated in this study have been deposited in the National Center for Biotechnology Information Gene Expression Omnibus (GEO) database (https://www.ncbi.nlm.nih.gov/geo) under the GEO series accession numbers GSE278129, GSE278130 and GSE278296. The immunoprecipitation mass spectrometry (IP-MS) data for heterochomatin-associated proteins and Nat10-interacting proteins in mESCs generated in this study are available via ProteomeXchange with the identifiers PXD056153 and PXD062677.

References

1. Arango D, Sturgill D, Alhusaini N *et al.* Acetylation of cytidine in mRNA promotes translation efficiency. *Cell* 2018;**175**:1872–86. https://doi.org/10.1016/j.cell.2018.10.030
2. Thomas G, Gordon J, Rogg H. N4-Acetylcytidine. A previously unidentified labile component of the small subunit of eukaryotic ribosomes. *J Biol Chem* 1978;**253**:1101–5. https://doi.org/10.1016/S0021-9258(17)38117-6
3. Zachau HG, Dutting D, Feldmann H. The structures of two serine transfer ribonucleic acids. *Hoppe Seylers Z Physiol Chem* 1966;**347**:212–35. https://doi.org/10.1515/bchm2.1966.347.1.212
4. Arango D, Sturgill D, Yang R *et al.* Direct epitranscriptomic regulation of mammalian translation initiation through N4-acetylcytidine. *Mol Cell* 2022;**82**:2912. https://doi.org/10.1016/j.molcel.2022.06.022
5. Balmus G, Larrieu D, Barros AC *et al.* Targeting of NAT10 enhances healthspan in a mouse model of human accelerated aging syndrome. *Nat Commun* 2018;**9**:1700. https://doi.org/10.1038/s41467-018-03770-3
6. Wang WJ, Wu YK, Liu SY *et al.* NAT10-mediated mRNA N4-acetylcytidine modifications in mouse oocytes constitute a

checkpoint of ovarian follicle development. *Sci Bull (Beijing)* 2024;**70**:837–41. https://doi.org/10.1016/j.scib.2024.09.020
7. Oh TI, Lee YM, Lim BO *et al.* Inhibition of NAT10 suppresses melanogenesis and melanoma growth by attenuating microphthalmia-associated transcription factor (MITF) expression. *Int J Mol Sci* 2017;**18**:1924. https://doi.org/10.3390/ijms18091924
8. Zheng X, Wang Q, Zhou Y *et al.* N-acetyltransferase 10 promotes colon cancer progression by inhibiting ferroptosis through N4-acetylation and stabilization of ferroptosis suppressor protein 1 (FSP1) mRNA. *Cancer Commun* 2022;**42**:1347–66. https://doi.org/10.1002/cac2.12363
9. Liao L, He Y, Li SJ *et al.* Lysine 2-hydroxyisobutyrylation of NAT10 promotes cancer metastasis in an ac4C-dependent manner. *Cell Res* 2023;**33**:355–71. https://doi.org/10.1038/s41422-023-00793-4
10. Deng M, Zhang L, Zheng W *et al.* Helicobacter pylori-induced NAT10 stabilizes MDM2 mRNA via RNA acetylation to facilitate gastric cancer progression. *J Exp Clin Cancer Res* 2023;**42**:9. https://doi.org/10.1186/s13046-022-02586-w
11. Wang L, Tao Y, Zhai J *et al.* The emerging roles of ac4C acetylation "writer" NAT10 in tumorigenesis: a comprehensive review. *Int J Biol Macromol* 2024;**254**:127789. https://doi.org/10.1016/j.ijbiomac.2023.127789
12. Mei Z, Shen Z, Pu J *et al.* NAT10 mediated ac4C acetylation driven m (6)A modification via involvement of YTHDC1-LDHA/PFKM regulates glycolysis and promotes osteosarcoma. *Cell Commun Signal* 2024;**22**:51. https://doi.org/10.1186/s12964-023-01321-y
13. Liu R, Wubulikasimu Z, Cai R *et al.* NAT10-mediated N4-acetylcytidine mRNA modification regulates self-renewal in human embryonic stem cells. *Nucleic Acids Res* 2023;**51**:8514–31. https://doi.org/10.1093/nar/gkad628
14. Hu Z, Lu Y, Cao J *et al.* N-acetyltransferase NAT10 controls cell fates via connecting mRNA cytidine acetylation to chromatin signaling. *Sci Adv* 2024;**10**:eadh9871. https://doi.org/10.1126/sciadv.adh9871
15. Evans MJ, Kaufman MH. Establishment in culture of pluripotential cells from mouse embryos. *Nature* 1981;**292**:154–6. https://doi.org/10.1038/292154a0
16. Martin GR. Isolation of a pluripotent cell line from early mouse embryos cultured in medium conditioned by teratocarcinoma stem cells. *Proc Natl Acad Sci USA* 1981;**78**:7634–8. https://doi.org/10.1073/pnas.78.12.7634
17. Maksakova IA, Thompson PJ, Goyal P *et al.* Distinct roles of KAP1, HP1 and G9a/GLP in silencing of the two-cell-specific retrotransposon MERVL in mouse ES cells. *Epigenetics Chromatin* 2013;**6**:15. https://doi.org/10.1186/1756-8935-6-15
18. Liu L. Linking telomere regulation to stem cell pluripotency. *Trends Genet* 2017;**33**:16–33. https://doi.org/10.1016/j.tig.2016.10.007
19. Dan J, Liu Y, Liu N *et al.* Rif1 maintains telomere length homeostasis of ESCs by mediating heterochromatin silencing. *Dev Cell* 2014;**29**:7–19. https://doi.org/10.1016/j.devcel.2014.03.004
20. Wu K, Liu H, Wang Y *et al.* SETDB1-mediated cell fate transition between 2C-Like and pluripotent states. *Cell Rep* 2020;**30**:25–36. https://doi.org/10.1016/j.celrep.2019.12.010
21. Macfarlan TS, Gifford WD, Driscoll S *et al.* Embryonic stem cell potency fluctuates with endogenous retrovirus activity. *Nature* 2012;**487**:57–63. https://doi.org/10.1038/nature11244
22. Young RA. Control of the embryonic stem cell state. *Cell* 2011;**144**:940–54. https://doi.org/10.1016/j.cell.2011.01.032
23. Chen L, Daley GQ. Molecular basis of pluripotency. *Hum Mol Genet* 2008;**17**:R23–7. https://doi.org/10.1093/hmg/ddn050
24. Li M, Liu GH, Izpisua Belmonte JC. Navigating the epigenetic landscape of pluripotent stem cells. *Nat Rev Mol Cell Biol* 2012;**13**:524–35. https://doi.org/10.1038/nrm3393
25. Lauria A, Meng G, Proserpio V *et al.* DNMT3B supports meso-endoderm differentiation from mouse embryonic stem cells. *Nat Commun* 2023;**14**:367. https://doi.org/10.1038/s41467-023-35938-x
26. Costa Y, Ding J, Theunissen TW *et al.* NANOG-dependent function of TET1 and TET2 in establishment of pluripotency. *Nature* 2013;**495**:370–4. https://doi.org/10.1038/nature11925
27. Bartoccetti M, van der Veer BK, Luo X *et al.* Regulatory dynamics of Tet1 and Oct4 resolve stages of global DNA demethylation and transcriptomic changes in reprogramming. *Cell Rep* 2020;**30**:3948. https://doi.org/10.1016/j.celrep.2020.03.015
28. De Iaco A, Planet E, Coluccio A *et al.* DUX-family transcription factors regulate zygotic genome activation in placental mammals. *Nat Genet* 2017;**49**:941–5. https://doi.org/10.1038/ng.3858
29. De Iaco A, Coudray A, Duc J *et al.* DPPA2 and DPPA4 are necessary to establish a 2C-like state in mouse embryonic stem cells. *EMBO Rep* 2019;**20**:e47382. https://doi.org/10.15252/embr.201847382
30. Hu Z, Tan DEK, Chia G *et al.* Maternal factor NELFA drives a 2C-like state in mouse embryonic stem cells. *Nat Cell Biol* 2020;**22**:175–86. https://doi.org/10.1038/s41556-019-0453-8
31. Adams IR, McLaren A. Identification and characterisation of mRif1: a mouse telomere-associated protein highly expressed in germ cells and embryo-derived pluripotent stem cells. *Dev Dyn* 2004;**229**:733–44. https://doi.org/10.1002/dvdy.10471
32. Yu H, Sun Z, Tan T *et al.* rRNA biogenesis regulates mouse 2C-like state by 3D structure reorganization of peri-nucleolar heterochromatin. *Nat Commun* 2021;**12**:6365. https://doi.org/10.1038/s41467-021-26576-2
33. Sun Z, Yu H, Zhao J *et al.* LIN28 coordinately promotes nucleolar/ribosomal functions and represses the 2C-like transcriptional program in pluripotent stem cells. *Protein Cell* 2022;**13**:490–512. https://doi.org/10.1007/s13238-021-00864-5
34. Xu W, Li J, He C *et al.* METTL3 regulates heterochromatin in mouse embryonic stem cells. *Nature* 2021;**591**:317–21. https://doi.org/10.1038/s41586-021-03210-1
35. Wei J, Yu X, Yang L *et al.* FTO mediates LINE1 m (6)A demethylation and chromatin regulation in mESCs and mouse development. *Science* 2022;**376**:968–73. https://doi.org/10.1126/science.abe9582
36. Guo R, Ye X, Yang J *et al.* Feeders facilitate telomere maintenance and chromosomal stability of embryonic stem cells. *Nat Commun* 2018;**9**:2620. https://doi.org/10.1038/s41467-018-05038-2
37. Zhang S, Huang F, Wang Y *et al.* NAT10-mediated mRNA N (4)-acetylcytidine reprograms serine metabolism to drive leukaemogenesis and stemness in acute myeloid leukaemia. *Nat Cell Biol* 2024;**26**:2168–82. https://doi.org/10.1038/s41556-024-01548-y
38. Ratnadiwakara M, Anko ML. mRNA stability assay using transcription inhibition by actinomycin D in mouse pluripotent stem cells. *Bio Protoc* 2018;**8**:e3072. https://doi.org/10.21769/BioProtoc.3072
39. Zhao N, Yin G, Liu C *et al.* Critically short telomeres derepress retrotransposons to promote genome instability in embryonic stem cells. *Cell Discov* 2023;**9**:45. https://doi.org/10.1038/s41421-023-00538-y
40. Dobin A, Gingeras TR. Mapping RNA-seq Reads with STAR. *Curr Protoc Bioinformatics* 2015;**51**:11.14.1–19. https://doi.org/10.1002/0471250953.bi1114s51
41. Liao Y, Smyth GK, Shi W. featureCounts: an efficient general purpose program for assigning sequence reads to genomic features. *Bioinformatics* 2014;**30**:923–30. https://doi.org/10.1093/bioinformatics/btt656
42. Love MI, Huber W, Anders S. Moderated estimation of fold change and dispersion for RNA-seq data with DESeq2. *Genome Biol* 2014;**15**:550. https://doi.org/10.1186/s13059-014-0550-8
43. Langmead B, Salzberg SL. Fast gapped-read alignment with Bowtie 2. *Nat Methods* 2012;**9**:357–9. https://doi.org/10.1038/nmeth.1923
44. Le R, Huang Y, Zhang Y *et al.* Dcaf11 activates Zscan4-mediated alternative telomere lengthening in early embryos and embryonic

stem cells. *Cell Stem Cell* 2021;**28**:732–47. https://doi.org/10.1016/j.stem.2020.11.018
45. Ramirez F, Dundar F, Diehl S *et al.* deepTools: a flexible platform for exploring deep-sequencing data. *Nucleic Acids Res* 2014;**42**:W187–91. https://doi.org/10.1093/nar/gku365
46. Thorvaldsdottir H, Robinson JT, Mesirov JP. Integrative Genomics Viewer (IGV): high-performance genomics data visualization and exploration. *Briefings Bioinf* 2013;**14**:178–92. https://doi.org/10.1093/bib/bbs017
47. Kim D, Langmead B, Salzberg SL. HISAT: a fast spliced aligner with low memory requirements. *Nat Methods* 2015;**12**:357–60. https://doi.org/10.1038/nmeth.3317
48. Tang Y, Chen K, Song B *et al.* m6A-Atlas: a comprehensive knowledgebase for unraveling the N6-methyladenosine (m6A) epitranscriptome. *Nucleic Acids Res* 2021;**49**:D134–43. https://doi.org/10.1093/nar/gkaa692
49. Heinz S, Benner C, Spann N *et al.* Simple combinations of lineage-determining transcription factors prime cis-regulatory elements required for macrophage and B cell identities. *Mol Cell* 2010;**38**:576–89. https://doi.org/10.1016/j.molcel.2010.05.004
50. Cui X, Wei Z, Zhang L *et al.* Guitar: an R/bioconductor package for gene annotation guided transcriptomic analysis of RNA-related genomic features. *Biomed Res Int* 2016;**2016**:8367534. https://doi.org/10.1155/2016/8367534
51. Yu G, Wang LG, He QY. ChIPseeker: an R/Bioconductor package for ChIP peak annotation, comparison and visualization. *Bioinformatics* 2015;**31**:2382–3. https://doi.org/10.1093/bioinformatics/btv145
52. Becker JS, McCarthy RL, Sidoli S *et al.* Genomic and proteomic resolution of heterochromatin and its restriction of alternate fate genes. *Mol Cell* 2017;**68**:1023–37. https://doi.org/10.1016/j.molcel.2017.11.030
53. Ji X, Dadon DB, Abraham BJ *et al.* Chromatin proteomic profiling reveals novel proteins associated with histone-marked genomic regions. *Proc Natl Acad Sci USA* 2015;**112**:3841–6. https://doi.org/10.1073/pnas.1502971112
54. Jiang ZY, Wu YK, Deng ZQ *et al.* PCBP1/2 and TDP43 Function as NAT10 Adaptors to Mediate mRNA ac (4)C Formation in Mammalian Cells. *Adv Sci* 2024;**11**:e2400133. https://doi.org/10.1002/advs.202400133
55. Sharma S, Langhendries JL, Watzinger P *et al.* Yeast Kre33 and human NAT10 are conserved 18S rRNA cytosine acetyltransferases that modify tRNAs assisted by the adaptor Tan1/THUMPD1. *Nucleic Acids Res* 2015;**43**:2242–58. https://doi.org/10.1093/nar/gkv075
56. Shen H, Yang M, Li S *et al.* Mouse totipotent stem cells captured and maintained through spliceosomal repression. *Cell* 2021;**184**:2843–59. https://doi.org/10.1016/j.cell.2021.04.020
57. Shen Q, Zheng X, McNutt MA *et al.* NAT10, a nucleolar protein, localizes to the midbody and regulates cytokinesis and acetylation of microtubules. *Exp Cell Res* 2009;**315**:1653–67. https://doi.org/10.1016/j.yexcr.2009.03.007
58. Fu H, Zhang W, Li N *et al.* Elevated retrotransposon activity and genomic instability in primed pluripotent stem cells. *Genome Biol* 2021;**22**:201. https://doi.org/10.1186/s13059-021-02417-9
59. Zhang B, Zheng H, Huang B *et al.* Allelic reprogramming of the histone modification H3K4me3 in early mammalian development. *Nature* 2016;**537**:553–7. https://doi.org/10.1038/nature19361
60. Jiang X, Cheng Y, Zhu Y *et al.* Maternal NAT10 orchestrates oocyte meiotic cell-cycle progression and maturation in mice. *Nat Commun* 2023;**14**:3729. https://doi.org/10.1038/s41467-023-39256-0
61. Akiyama T, Xin L, Oda M *et al.* Transient bursts of Zscan4 expression are accompanied by the rapid derepression of heterochromatin in mouse embryonic stem cells. *DNA Res* 2015;**22**:307–18. https://doi.org/10.1093/dnares/dsv013
62. Hormoz S, Singer ZS, Linton JM *et al.* Inferring cell-state transition dynamics from lineage trees and endpoint single-cell measurements. *Cell Syst* 2016;**3**:419–33. https://doi.org/10.1016/j.cels.2016.10.015
63. Ito S, Horikawa S, Suzuki T *et al.* Human NAT10 is an ATP-dependent RNA acetyltransferase responsible for N4-acetylcytidine formation in 18 S ribosomal RNA (rRNA). *J Biol Chem* 2014;**289**:35724–30. https://doi.org/10.1074/jbc.C114.602698
64. Xie L, Zhong X, Cao W *et al.* Mechanisms of NAT10 as ac4C writer in diseases. *Mol Ther* 2023;**32**:359–68. https://doi.org/10.1016/j.omtn.2023.03.023
65. Furusawa T, Ohkoshi K, Honda C *et al.* Embryonic stem cells expressing both platelet endothelial cell adhesion molecule-1 and stage-specific embryonic antigen-1 differentiate predominantly into epiblast cells in a chimeric embryo. *Biol Reprod* 2004;**70**:1452–7. https://doi.org/10.1095/biolreprod.103.024190
66. Hayashi K, de Sousa Lopes SMC, Tang F *et al.* Dynamic equilibrium and heterogeneity of mouse pluripotent stem cells with distinct functional and epigenetic states. *Cell Stem Cell* 2008;**3**:391–401. https://doi.org/10.1016/j.stem.2008.07.027
67. Zhao W, Zhou Y, Cui Q *et al.* PACES: prediction of N4-acetylcytidine (ac4C) modification sites in mRNA. *Sci Rep* 2019;**9**:11112. https://doi.org/10.1038/s41598-019-47594-7
68. Larrieu D, Britton S, Demir M *et al.* Chemical inhibition of NAT10 corrects defects of laminopathic cells. *Science* 2014;**344**:527–32. https://doi.org/10.1126/science.1252651
69. Dan J, Li M, Yang J *et al.* Roles for Tbx3 in regulation of two-cell state and telomere elongation in mouse ES cells. *Sci Rep* 2013;**3**:3492. https://doi.org/10.1038/srep03492
70. Lu F, Liu Y, Jiang L *et al.* Role of Tet proteins in enhancer activity and telomere elongation. *Genes Dev* 2014;**28**:2103–19. https://doi.org/10.1101/gad.248005.114
71. Deng L, Ren R, Liu Z *et al.* Stabilizing heterochromatin by DGCR8 alleviates senescence and osteoarthritis. *Nat Commun* 2019;**10**:3329. https://doi.org/10.1038/s41467-019-10831-8
72. Kobylecki K, Drazkowska K, Kulinski TM *et al.* Elimination of 01/A'-A0 pre-rRNA processing by-product in human cells involves cooperative action of two nuclear exosome-associated nucleases: RRP6 and DIS3. *RNA* 2018;**24**:1677–92. https://doi.org/10.1261/rna.066589.118
73. Percharde M, Lin CJ, Yin Y *et al.* A LINE1-nucleolin partnership regulates early development and ESC identity. *Cell* 2018;**174**:391–405. https://doi.org/10.1016/j.cell.2018.05.043
74. Lu JY, Shao W, Chang L *et al.* Genomic repeats categorize genes with distinct functions for orchestrated regulation. *Cell Rep* 2020;**30**:3296–311. https://doi.org/10.1016/j.celrep.2020.02.048
75. Liu J, Gao M, He J *et al.* The RNA m (6)A reader YTHDC1 silences retrotransposons and guards ES cell identity. *Nature* 2021;**591**:322–6. https://doi.org/10.1038/s41586-021-03313-9
76. Chen C, Liu W, Guo J *et al.* Nuclear m (6)A reader YTHDC1 regulates the scaffold function of LINE1 RNA in mouse ESCs and early embryos. *Protein Cell* 2021;**12**:455–74. https://doi.org/10.1007/s13238-021-00837-8
77. Nichols J, Smith A. Naive and primed pluripotent states. *Cell Stem Cell* 2009;**4**:487–92. https://doi.org/10.1016/j.stem.2009.05.015
78. Tesar PJ, Chenoweth JG, Brook FA *et al.* New cell lines from mouse epiblast share defining features with human embryonic stem cells. *Nature* 2007;**448**:196–9. https://doi.org/10.1038/nature05972
79. Brons IG, Smithers LE, Trotter MW *et al.* Derivation of pluripotent epiblast stem cells from mammalian embryos. *Nature* 2007;**448**:191–5. https://doi.org/10.1038/nature05950
80. Debnath TK, Abell NS, Li YR *et al.* NAT10 and N (4)-acetylcytidine restrain R-loop levels and related inflammatory responses. *Sci Adv* 2025;**11**:eads6144. https://doi.org/10.1126/sciadv.ads6144
81. Torres-Padilla ME. On transposons and totipotency. *Phil Trans R Soc B* 2020;**375**:20190339. https://doi.org/10.1098/rstb.2019.0339

82. Eckersley-Maslin MA, Alda-Catalinas C, Reik W. Dynamics of the epigenetic landscape during the maternal-to-zygotic transition. *Nat Rev Mol Cell Biol* 2018;**19**:436–50. https://doi.org/10.1038/s41580-018-0008-z
83. Yang M, Yu H, Yu X *et al.* Chemical-induced chromatin remodeling reprograms mouse ESCs to totipotent-like stem cells. *Cell Stem Cell* 2022;**29**:400–18. https://doi.org/10.1016/j.stem.2022.01.010
84. Fu H, Tian CL, Ye X *et al.* Dynamics of telomere rejuvenation during chemical induction to pluripotent stem cells. *Stem Cell Rep* 2018;**11**:70–87. https://doi.org/10.1016/j.stemcr.2018.05.003

Received: November 27, 2024. **Revised:** May 22, 2025. **Editorial Decision:** May 23, 2025. **Accepted:** May 28, 2025